Chapter 2
Component Tests

2.1 Overview

Component tests were performed with the aim of characterizing the behaviour of both beam-to-upright and base connections, in order to allow a correct interpretation of full scale tests as well as in order to calibrate numerical models. It has to be noticed that the behaviour of both components is strongly influenced by the following factors:

- Nature and geometry of the profiles (unsymmetrical cross section of the upright, thin walled sections of both beams and uprights, see Fig. 2.1)
- Asymmetry of the connections. In the case of the beam-to-upright connection, the asymmetry is caused by the inclined hooks and by the presence of the safety-bolt on the upper side of the beam end-plate connector only (Fig. 2.2a). In the case of the base connections, the asymmetry is due to the eccentric position of the upright on the base-plate, and by the asymmetrical disposition of the bolts (Fig. 2.2b).

Special attention was paid to component and connections testing procedures presented in Chap. 5 ("Tests") of FEM 10.2.02 (2001): *The Design of Static Steel Pallet Racks*, namely:

- 5.5—Bending tests on beam end connections
- 5.8—Tests on floor connections

Based on such specifications the following tests were performed at the Laboratory for Testing Materials of the Civil Engineering and Architecture Department of Instituto Superior Tecnico of Lisbon, by the team leaded by prof. L. Calado, and in co-ordination with this author, who attended the tests in two occasions, in November 2005 and in January 2006.

C.A. Castiglioni, *Seismic Behavior of Steel Storage Pallet Racking Systems*,
Research for Development, DOI 10.1007/978-3-319-28466-8_2

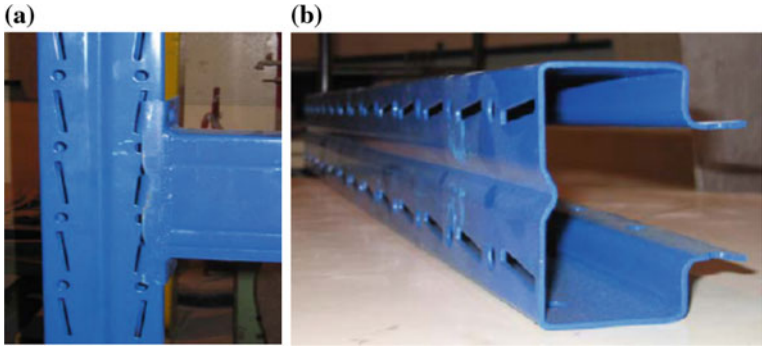

Fig. 2.1 Specimens for beam-to-upright connection tests: **a** connection, **b** upright (100/20b)

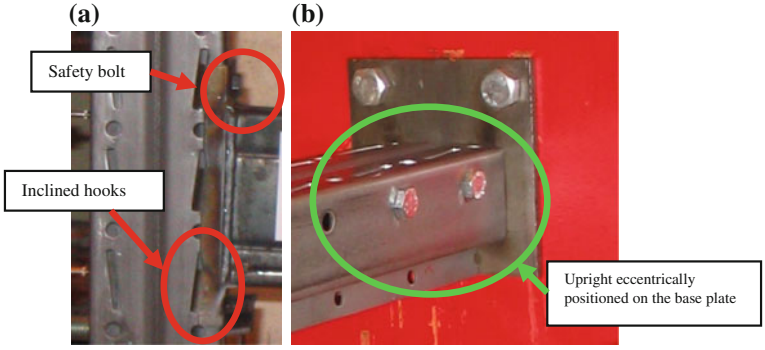

Fig. 2.2 Asymmetries in the connections: **a** beam-to-upright, **b** bases

2.2 Beam-to-Upright Connections

Proprietary moment connections are typically used as beam-to-upright connections for steel selective pallet storage racks. This study focused on the beam-to-upright connection type shown in Fig. 2.3. A "hooked" end plate connector is welded to the beam at both ends. Connection is attained by introducing the hooks in the openings (punched during fabrication) on the uprights, and by adding a safety bolt connecting the upper part of the extended end-plate to the upright.

As a general remark, it should be noticed that this proprietary beam-to-upright connection is strongly non-symmetric in both vertical and horizontal planes.

In the vertical plane, non-symmetry is due to the presence of the safety bolt on the upper side of the beam only (Fig. 2.3) and by the fact that the beam is fillet welded to the end-plate on three sides only, leaving the lower flange un-welded.

In the horizontal plane, non-symmetry is due to the shape of the end-plate connector that has hooks on one side only, and is obtained by cold forming of a thin plate, bent in shape of an L, so with a stiffened edge (the same edge where hooks are present).

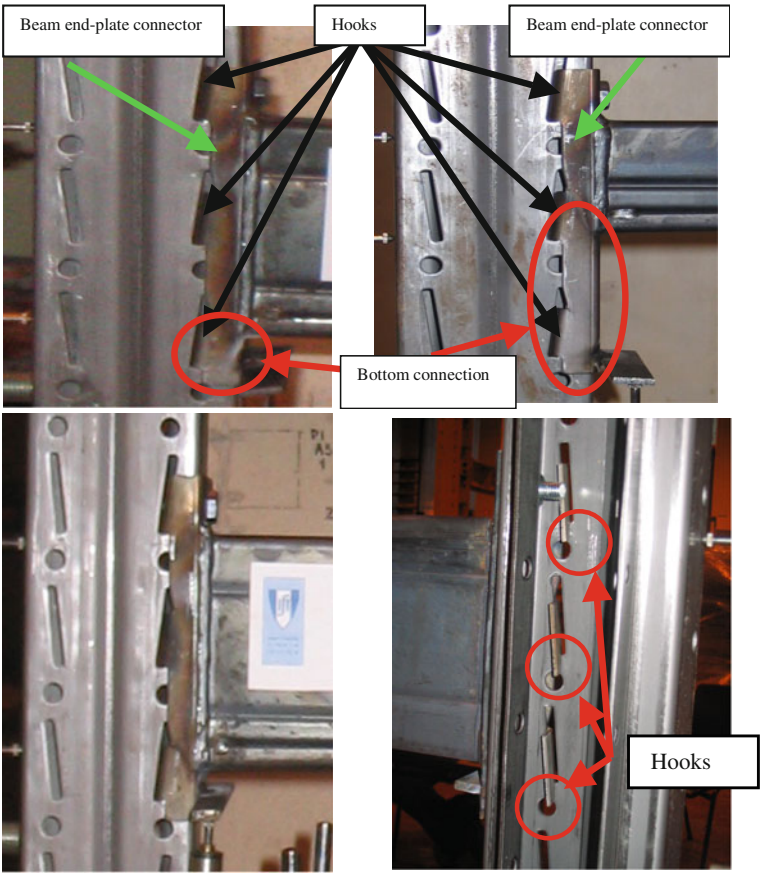

Fig. 2.3 Typical beam-to-upright connection considered in the study

A non-symmetric response is hence to be expected under hogging and sagging bending.

Objectives of the tests were:

- Assessment of the moment-rotation curves.
- Assessment of the collapse modes of these connections under monotonic and cyclic loads.

Two different cross-section for beams (TG 70 × 45 × 1.5 and TG 130 × 45 × 1.5 mm) were adopted (Fig. 2.4), with upright of identical cross-section (100/20b) shown in Fig. 2.1b. Consequently, beam height varied between 70 and 130 mm. The member geometrical properties are shown in Table 2.1.

The material used for beams and upright is S275 steel, with actual values of yield and ultimate stress showed in Table 2.2.

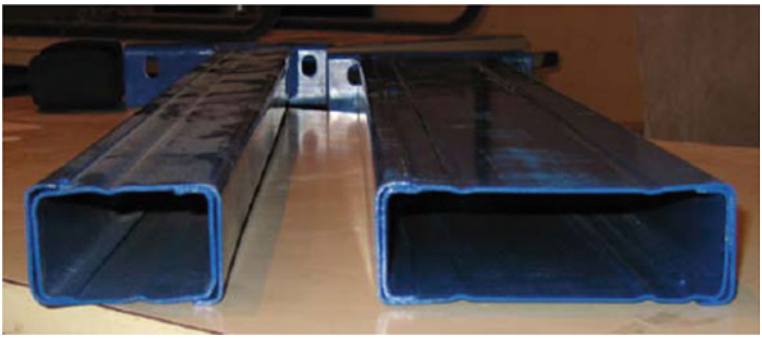

Fig. 2.4 Types of beams (70 × 45 × 1.5 and 130 × 45 × 1.5)

Table 2.1 Geometrical properties of the members

Member	Properties	Gross section	Net section
100/20b	A [mm^2]	588.8	525.7
	t [mm]	2.0	2.0
	J_x [mm^4]	436020	406100
	J_y [mm^4]	812280	694680
	W_x [mm^3]	8543	8330
	W_y [mm^3]	16747	14323
TG 70 × 45 × 1.5 mm	A [mm^2]	514.06	514.06
	t [mm]	1.5	1.5
	J_x [mm^4]	407500	407500
	J_y [mm^4]	136272	136272
	W_x [mm^3]	11754	11754
	W_y [mm^3]	4764	4764
TG 130 × 45 × 1.5 mm	A [mm^2]	697.66	697.66
	t [mm]	1.5	1.5
	J_x [mm^4]	1742220	1742220
	J_y [mm^4]	168662	168662
	W_x [mm^3]	26792	26792
	W_y [mm^3]	5171	5171

Table 2.2 Material characteristics

Member	f_y [MPa]	f_u [MPa]	ε_u [%]
Beam 70 × 45 × 1.5	353.6	446.1	26.90
Beam 130 × 45 × 1.5	357.0	458.0	27.00
Upright 100 × 82 × 2.0	348.0	493.0	25.50
Beam end connector	263.0	385.0	41.10

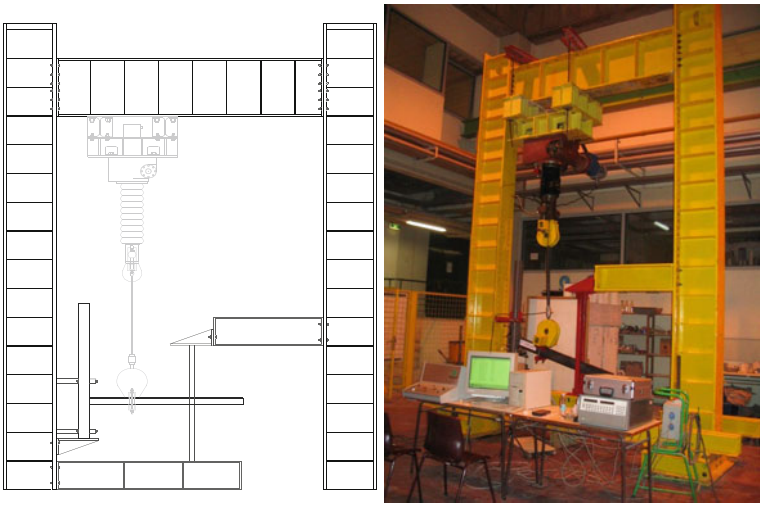

Fig. 2.5 Test set up

The test set-up and instrumentation are shown in the following Figs. 2.5 and 2.6. Specimen size, configuration and instrumentation (Figs. 2.6 and 2.7) were adopted according to FEM 10.2.02 (2001) Recommendations.

The moment-rotation curves were plotted for each test. The bending moment was defined as $(M = F * a)$ and the rotation of the connection by Eq. (2.1).

$$\phi = \frac{V}{a} - \left(\frac{\delta_1 - \delta_2}{d}\right) \tag{2.1}$$

where (see Fig. 2.7):

V displacement due to load F;
a lever arm for the load F;
δ_1 deflection measured by transducer T1;
δ_2 deflection measured by transducer T2;
d beam height.

Table 2.3 summarizes and identifies the 30 tests carried out on beam-to-upright specimens. In particular, monotonic tests were performed under both hogging (MB) and sagging (MT) bending moments.

As the Standard cyclic testing procedure proposed by ECCS (1986), in particular in the case of unsimmetric behaviour (as in the case under exam), leads to a correct evaluation of the cyclic behaviour of components only for the condition of unloaded structure (vertical load F = 0), an innovative cyclic testing procedure has been identified and applied.

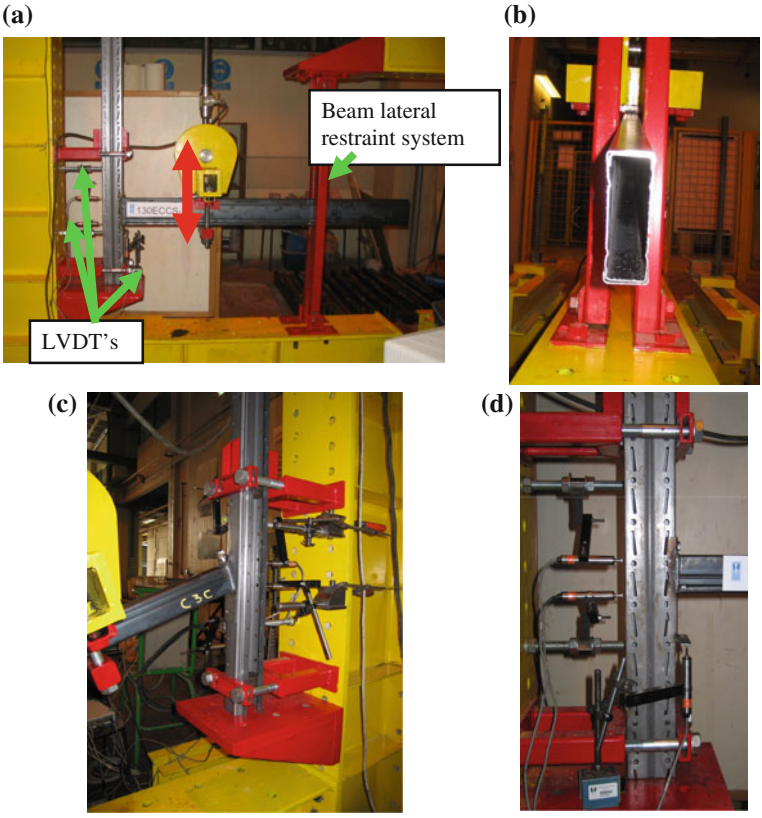

Fig. 2.6 Test set up, **a** test sut-up, **b** lateral restraint system, **c**, **d** instrumentation

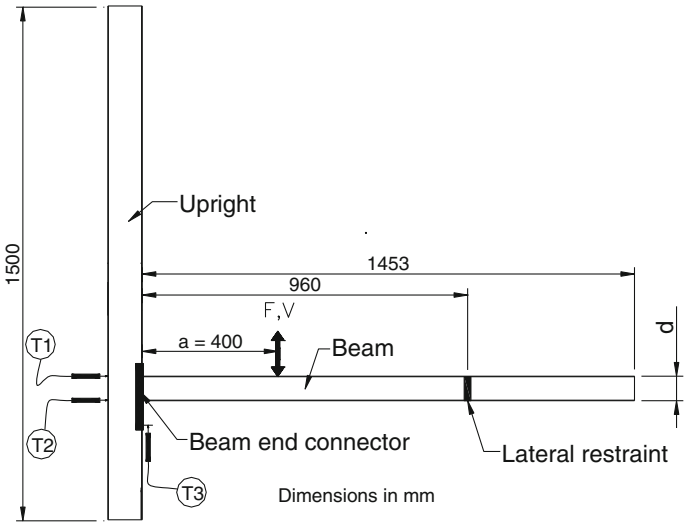

Fig. 2.7 Specimen dimensions and instrumentation

Table 2.3 Tests on beam-to-upright connections

TEST	Beam width—70 mm	Beam width—130 mm
Monotonic—below (hogging bending)	70MB-1 70MB-3 70MB-4	130MB-2 130MB-3 130MB-4
Monotonic—top (sagging bending)	70MT-3 70MT-5 70MT-6	130MT-2 130MT-3 130MT-5
Cyclic—ECCS	70ECCS-1 70ECCS-2	130ECCS-2 130ECCS-3
Cyclic—Fy25	70Fy25-3 70Fy25-4	130Fy25-1 130Fy25-2
Cyclic—Fy50	70Fy50-1 70Fy50-2	130Fy50-1 130Fy50-2
Cyclic—Fy66	70Fy66-1 70Fy66-2	130Fy66-1 130Fy66-2
Cyclic—Fy75	70Fy75-1	130Fy75-1

Hence, cyclic tests were carried out under different levels of vertical load (namely 0, 25, 50, 66 and 75 of the yield load F_y of the connection) in order to simulate the presence of a service gravity load on the beam.

The yield strength F_y, as well as other relevant parameters, such as the yield displacement v_y, the ultimate strength F_u, as well as the ultimate displacement v_u, and the initial elastic stiffness $S_{j,ini}$, can be conventionally defined according to ECCS (1986), with reference to the results of a monotonic test (Fig. 2.8).

2.2.1 Monotonic Tests

2.2.1.1 Beam 70 × 45 × 1.5

The monotonic tests listed in Table 2.4 were carried out on beam-to-upright connections specimens with beam 70 × 45 × 1.5 mm.

Table 2.4 reports also the values of the yield (M_y) and ultimate bending moment (M_u), of the yield (ϕ_y) and ultimate rotation (ϕ_u) and of the initial elastic stiffness ($S_{j,ini}$) measured for each test, as well as the mean values of the same parameters.

Figure 2.9 compares the moment-rotation curves for both hogging (MB) and sagging (MT) bending, in the case of beam 70 × 45 × 1.5. It can be noticed that the specimens under hogging bending show a slightly larger ultimate strength than the specimens under sagging bending moments, but about the same yield strength. The ductile behaviour is quite different: while the initial elastic stiffness is similar, the average ultimate rotation of the specimens under hogging bending is approximately 2.3 times larger than that of the specimens under sagging bending.

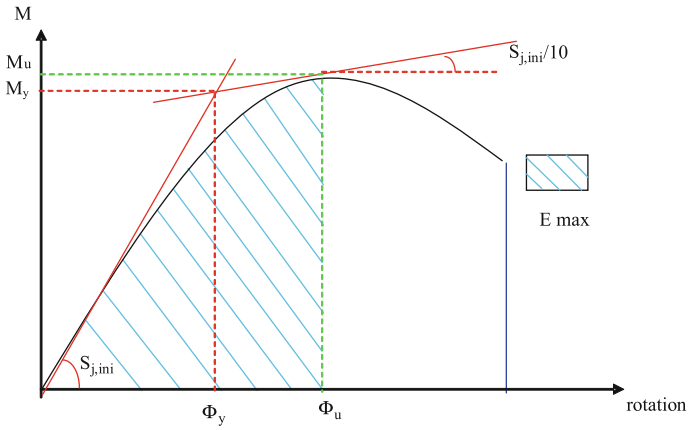

Fig. 2.8 Conventional definitions according to ECCS (1986)

Table 2.4 Monotonic tests on beam-to-upright connections with 70 × 45 × 1.5 mm beam

Loading	Specimen	M_y [kNm]	ϕ_y [mrad]	$S_{j,ini}$ [kNm/rad]	M_u [kNm]	ϕ_u [mrad]
Hogging bending	70MB-1	1.30	34.7	42.7	1.58	143
	70MB-3	1.22	26.0	48.7	1.68	191
	70MB-4	1.18	22.7	52.4	1.53	202
	Average	**1.23**	**27.8**	**47.9**	**1.60**	**178.7**
Sagging bending	70MT-3	1.27	27.3	46.0	1.44	86
	70MT-5	1.20	24.0	49.4	1.37	76
	70MT-6	1.26	26.7	51.3	1.44	71
	Average	**1.24**	**26.0**	**48.9**	**1.42**	**77.7**

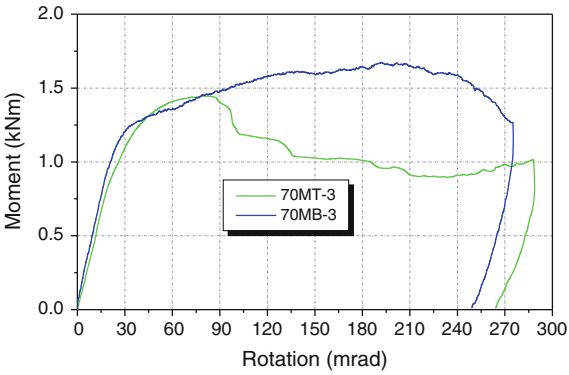

Fig. 2.9 Comparison of the moment-rotation curves for beam 70 × 45 × 1.5

This large difference can be explained (Figs. 2.10 and 2.11) by the presence of the extended end-plate connector (which has a standard size, and is the same for 70 mm as well as for 130 mm deep beams), by its unsymmetrical connection to the beam and by the presence of the safety bolt on the upper side of the beam only. All these factors cause an unsymmetrical behaviour of the connection for hogging and sagging bending moments. The failure mode of MB specimens, subjected to hogging bending, consisted of large deformations in the top zone of the beam end connector, leading to loosening of the hooked connection, with the hooks exiting from the holes in the upright.

The failure mode of MT specimens subjected to sagging bending was the fracture of the beam close to the weld between the beam and the end connector. Typical failure modes observed during the monotonic tests are presented in Figs. 2.10 and 2.11. For all tests the connection behaviour was not influenced by bolt deformation.

Fig. 2.10 Monotonic tests on beam-to-upright connections with 70 × 45 × 1.5 mm beam. Typical collapse mode under hogging bending moments

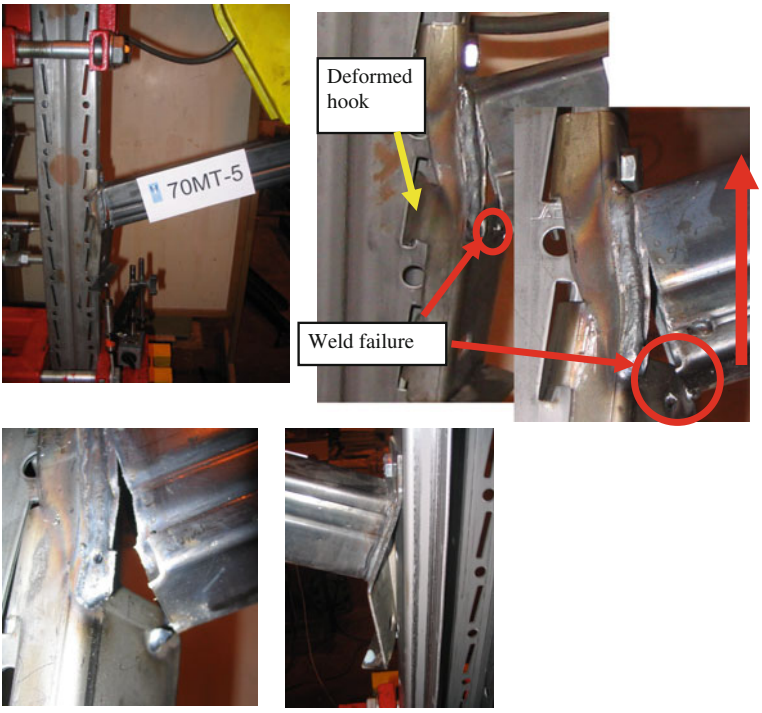

Fig. 2.11 Monotonic tests on beam-to-upright connections with 70 × 45 × 1.5 mm beam. Typical collapse mode under sagging bending moments

2.2.1.2 Beam 130 × 45 × 1.5

The monotonic tests carried out on beam-to-upright connections specimens with beam 130 × 45 × 1.5 mm are listed in Table 2.5.

Table 2.5 reports also the values of the yield (M_y) and ultimate bending moment (M_u), of the yield (ϕ_y) and ultimate rotation (ϕ_u) and of the initial elastic stiffness ($S_{j,ini}$) measured for each test, as well as the mean values of these parameters.

Figure 2.12 compares the moment-rotation curves for both hogging (MB) and sagging (MT) bending, in the case of beam 130 × 45 × 1.5. It can be noticed that the specimens under hogging bending show larger strength (M_u) and ultimate rotation (ϕ_u), but lower initial elastic stiffness ($S_{j,ini}$) than the specimens under sagging bending moments. This difference can be explained observing the following Figs. 2.13 and 2.14, presenting typical failure modes observed during the monotonic tests.

Failure of both specimens subjected to hogging (MB) and sagging (MT) bending was due to large deformations in the beam end connector, respectively resulting in the top and bottom hooks coming out of the openings in the upright.

Table 2.5 Monotonic tests on 130 × 45 × 1.5 mm beam specimens

Loading	Specimen	M_y [kNm]	ϕ_y [mrad]	$S_{j,ini}$ [kNm/rad]	M_u [kNm]	ϕ_u [mrad]
Hogging bending	130MB-2	2.52	23.0	101.9	3.18	122
	130MB-3	2.59	27.9	94.6	3.19	127
	130MB-4	2.49	27.1	90.9	3.05	140
	Average	**2.53**	**26.0**	**95.8**	**3.14**	**129.7**
Sagging bending	130MT-2	1.99	18.2	109.7	2.26	111
	130MT-3	2.22	18.6	122.2	2.63	97
	130MT-5	2.11	19.7	125.0	2.46	114
	Average	**2.11**	**18.8**	**119.0**	**2.44**	**107.3**

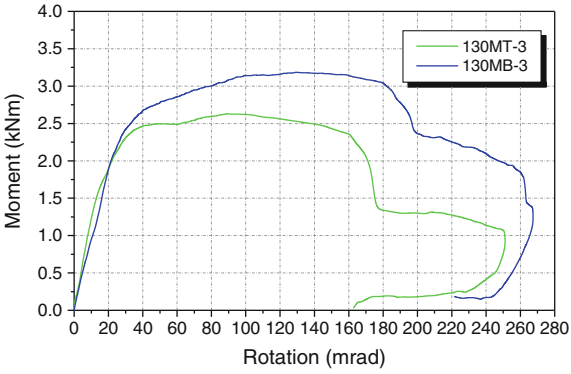

Fig. 2.12 Comparison of the moment-rotation curves for beam 130 × 45 × 1.5

Under hogging bending (Fig. 2.13) the safety bolt is in tension. Until it is completely punched through the hole in the end-plate connector, the presence of the bolt restrains the deformation of the upper part of the end-plate. Hence, only the upper hook can come out of the opening. On the contrary, under sagging bending, the collapse mechanism is governed by the failure of the hooks in the lower part of the end-plate connector. The openings on the uprights are inclined. This causes a different hook-opening interaction, in the case of hogging bending and of sagging bending. In this last case, in fact, due to a larger deformation sustained by the hooks, failure is attained with evident cracks in the hooks (Fig. 2.15).

2.2.2 Cyclic Tests

2.2.2.1 Cyclic Loading History

The seismic behaviour of beam-to-upright connections of racking systems is similar to that of more common beam-to-column connections of conventional reinforced

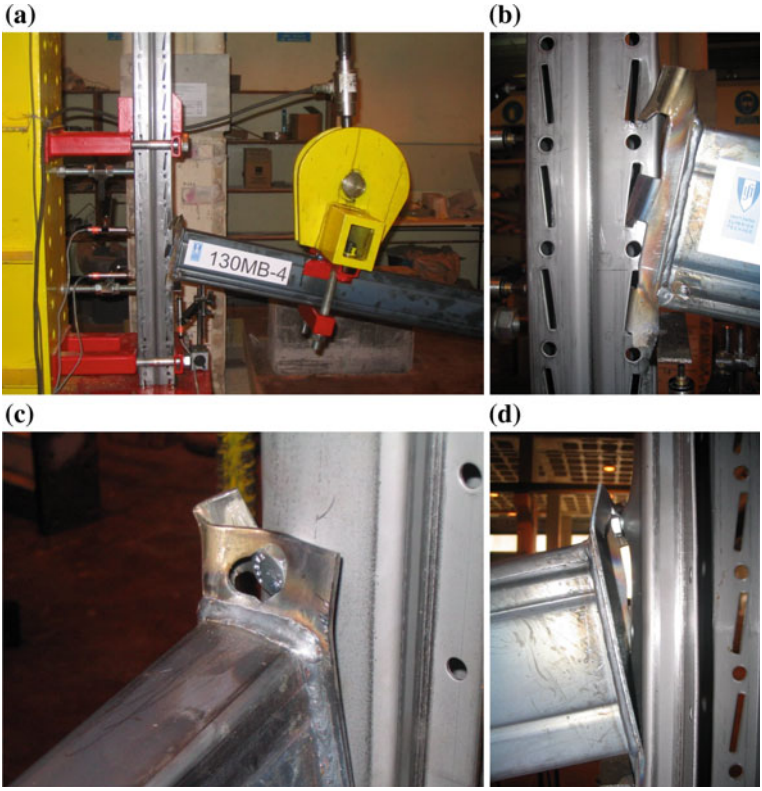

Fig. 2.13 Monotonic tests on beam-to-upright connections with 130 × 45 × 1.5 mm beam. Typical collapse mode under hogging bending moments

concrete or steel buildings. These more common structural sub-assemblages are generally tested with reference to recommendations available in the literature, such as those produced by ECCS (1986), ACI (1999) and ATC (1992). All these recommendations share the same basic characteristics listed hereafter:

Tests are displacement-controlled;
Specimens are subjected to a symmetrical reversed cyclic displacement history;
Displacement history is expressed in terms of imposed displacement ductility, making reference to the yield displacement, generally evaluated through monotonic tests;
Loading cycles are repeated at every displacement amplitude in the post-elastic range;
Failure is conventionally defined.

The positive and negative cycle amplitudes are based upon the following series:

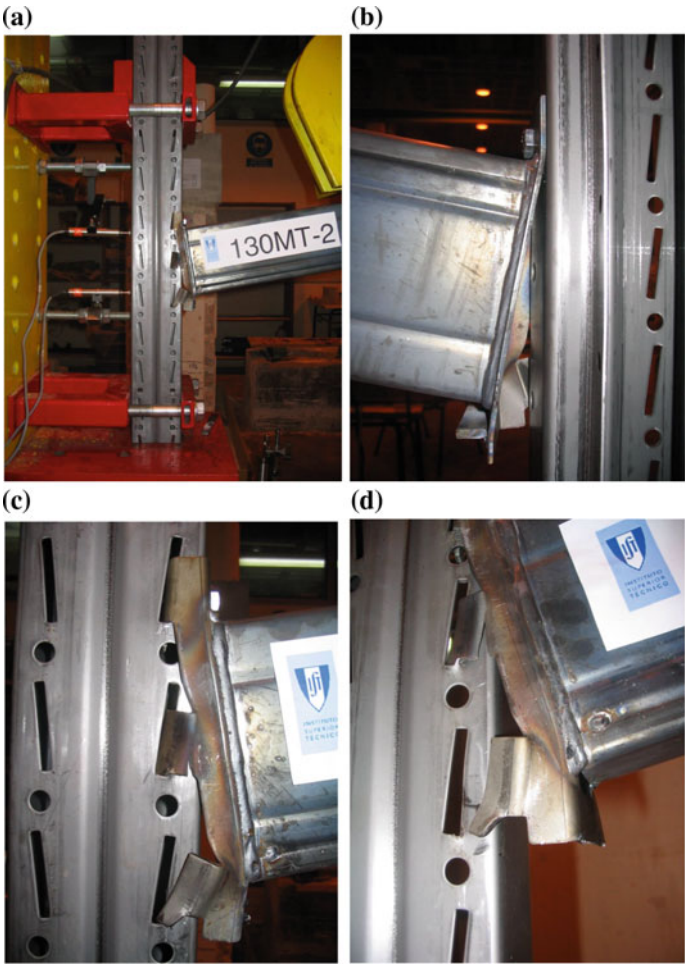

Fig. 2.14 Monotonic tests on beam-to-upright connections with 130 × 45 × 1.5 mm beam. Typical collapse mode under sagging bending moments

one cycle in the $d_y^+/4$, $d_y^-/4$ interval;
one cycle in the $2d_y^+/4$, $2d_y^-/4$ interval;
one cycle in the $3d_y^+/4$, $3d_y^-/4$ interval;
one cycle in the d_y^+, d_y^- interval;

two or three cycle in the $(2+n)d_y^+$, $(2+n)d_y^-$ interval with n = 0, 1, 2, 3, … until failure occurs.

These generally accepted recommendations served as a common ground for the comparison of different testing programmes (e.g. see Proença et al. 1994), as well as for the calibration of nonlinear numerical models and derivation of detailing rules

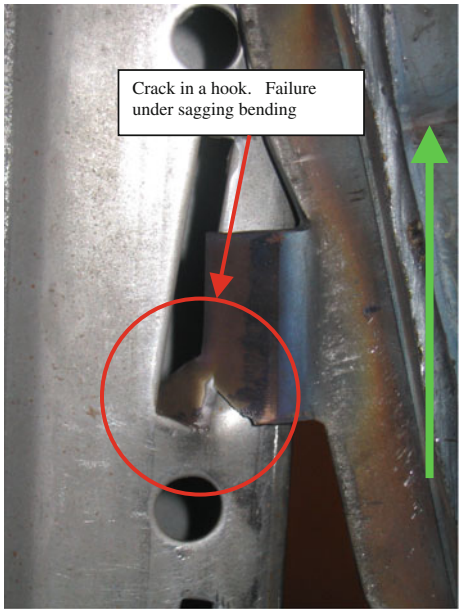

Fig. 2.15 Crack in a hook, at failure under sagging bending

for codes and other comparable documents. General performance indexes—such as available displacement ductility, strength/stiffness degradation and hysteretic energy-dissipation characteristics—can readily be inferred from cyclic tests carried out with reference to these recommendations.

In reality, the seismic behaviour of beam-to-upright connections of racking systems and, more in general, of beam-to-column connections in conventional r.c. or steel buildings is determined by a hybrid loading consisting of vertical (gravity) loads and horizontal (seismic) motion effects, and the beam-to-column connections bending moments are shifted in the negative, hogging, direction as a consequence of the vertical load effects. Failure occurs when the critical sections are no longer able to withstand vertical loads as a consequence of accumulated damage (induced by horizontal motion and vertical forces acting together).

However, general recommended testing procedures, encompassing only displacement controlled conditions, fail to address the unsymmetrical displacement histories experienced by critical beam-to-column connections when subjected to earthquake motion acting simultaneously with vertical (live and dead) loads.

2.2.2.1.1 Innovative Cyclic Testing Procedure

Considering the former limitations of the commonly accepted testing procedures (particularly evident when testing is performed in the inverted T configuration, with the beam standing vertically and the column horizontally), an innovative testing procedure was developed, which intends to capture the hybrid nature of loading

imposed to beam-to-column connections when subjected to vertical and horizontal load effects.

This innovative testing procedure can be considered a development of the commonly accepted testing procedures as it inherits some of their characteristics, such as the cycle repetition in the post-elastic range and the fact that the controlled-displacement part of the testing cycles is indexed to the yield displacement (determined through monotonic tests).

Gravitational load effects are expressed through F_g which can in turn be expressed as a fraction of the force leading to yielding (F_y) at the critical cross section of the connection. Values of F_g corresponding to 25, 50, 66 and 75 % of the yield force (F_y) were considered in the beam-to-upright testing programme. F_y can be determined by a monotonic test.

The testing procedure is composed by single fully reversed cycles at displacement ductility of 1/4, 1/2, 3/4 and 1, followed by a sequence of groups of two (or three) cycles at multiples (2, 3, 4, etc.) of the yield displacement until a conventional failure criterion is met.

Each cycle has an initial force-controlled part and a final displacement-controlled part.

In what follows, the gravity force is considered to be positive. As a consequence of this conventional choice, the "positive" bending moments are those associated with "hogging" bending.

Figure 2.16 depicts typical positive and negative succeeding cycles.

A typical *positive* cycle is composed of the following two parts:

Application of the force correspondent to vertical (gravitational) load effects F_g on the beam-to-column connection (force-controlled part of the cycle);

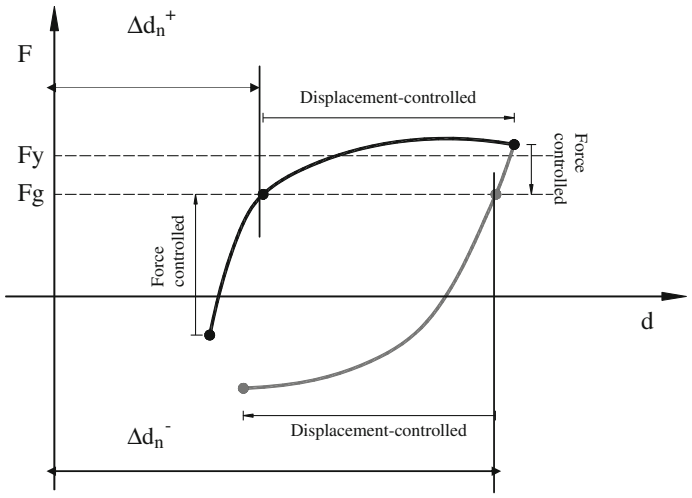

Fig. 2.16 Typical positive and subsequent negative cycles (positive forces induce hogging bending moments in the beam-to-column connection)

Starting from the displacement attained at the end of the force-controlled part of the cycle (Δd_n^+) the displacement controlled part of the cycle is imposed. The displacement amplitude is considered a multiple of the yield displacement.

Also the following *negative* cycle is composed of two different parts:

Force-controlled unloading until attainment of the force F_g associated with the presence of the vertical (gravity) loads alone;

Starting from the displacement (Δd_n^-) reached at the end of the force-controlled part of the cycle, the displacement-controlled part of the cycle is imposed to the specimen, until the intended displacement amplitude is reached.

The positive and negative cycles (in the post-elastic range) can be derived from the following equation:

$$\left((2+n)d_y^+ + \Delta d_n^+\right), \left((2+n)d_y^- + \Delta d_n^-\right) \quad (n = 0, 1, 2, 3, \ldots.)$$

where:

Δd_n displacement amplitude value obtained when the force-controlled part of the cycle reaches the force correspondent to gravitational load (F_g).

Adopting this innovative cyclic testing procedure, failure can be identified in one of the following situations:

When, in the force-controlled part of the positive cycle, the specimen fails to develop the force correspondent to gravitational loads (Fig. 2.17a).

When, in the displacement-controlled part of the positive cycle, the restoring force decreases to values below those corresponding to gravitational loads (Fig. 2.17b).

Obviously, failure can also occur in any of the positive or negative cycles when cross-sectional collapse occurs.

2.2.2.1.2 Comparison Between Testing Procedures

A comparison between the results obtainable by means of the ECCS and of the "innovative" testing procedure is presented hereafter, in the case of tests on 130 × 45 × 1.5 mm beams, without compromising the generality of the conclusions.

ECCS-type cyclic tests results can be exemplified in Fig. 2.18, which shows the force-displacement chart for specimen 130ECCS-2. The force-displacement chart is almost symmetrical with some slight differences in the positive and negative strength, which result from unsymmetrical detailing of the beam-to-upright connection. Low values of stiffness during most of the duration of these tests (as a consequence of the connection remaining fully opened) led to pronounced pinching effects.

Application of the innovative cyclic testing procedure led to a displacement history that could not be predicted *a priori* as a consequence of the force-controlled part of the cycles. Loading histories applied in tests with different values of F_g are different, as depicted in Fig. 2.19.

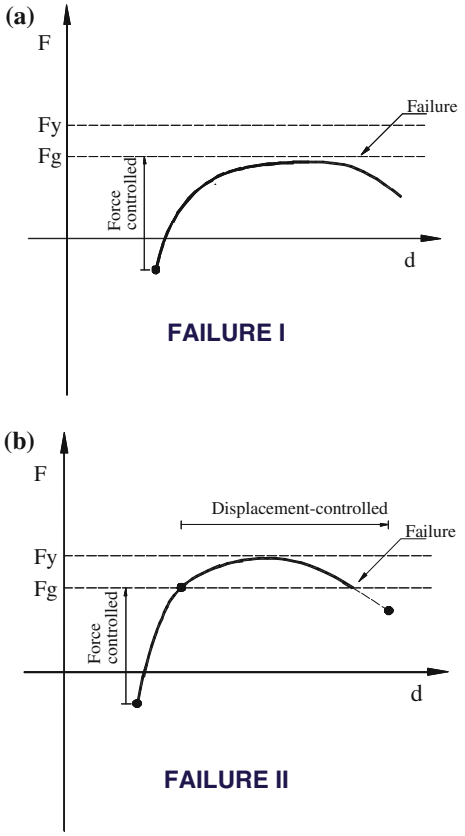

Fig. 2.17 Possible failure of specimen

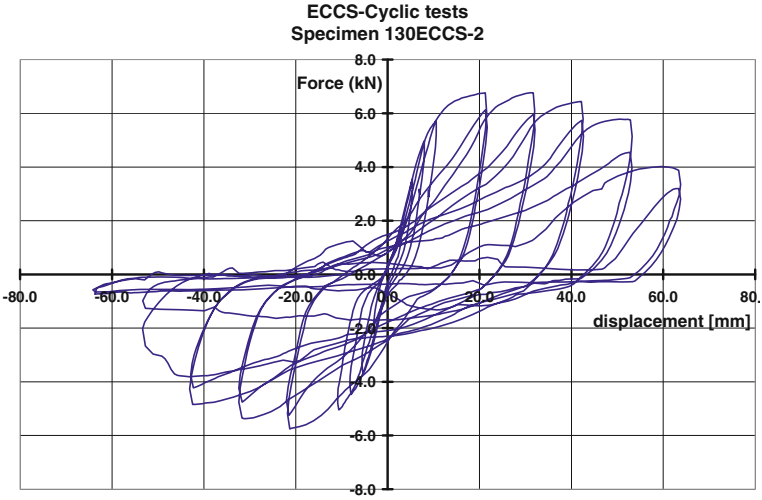

Fig. 2.18 ECCS cyclic test results for 130 mm height beam specimen

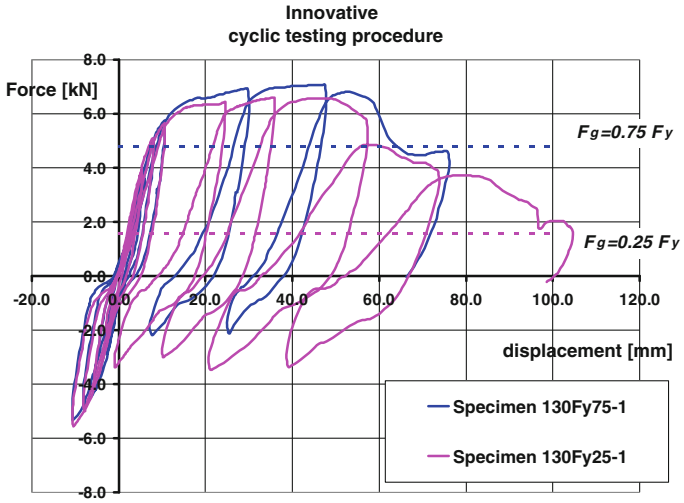

Fig. 2.19 Innovative cyclic testing procedure results for tests 130Fy25-1 and 130Fy75-1

In test 130Fy25-1 the specimen was subjected to elastic cycles, after which it endured two cycles of ±2 and 4 times d_y (d_y being the yield displacement) and failure occurred in the first positive 6 d_y displacement cycle. In test 130Fy75-1 the specimen failed in the first positive cycle with 4 d_y amplitude. The first, elastic, cycles are similar in both tests.

These two test results (as all the remaining tests conducted with the innovative cyclic testing procedure) are fundamentally different from those obtained through the application of the ECCS recommended testing procedure. Among the others, the following differences could be identified:

Imposed displacement history is unsymmetrical in the tests performed according to the innovative cyclic testing procedure. Displacements tend to systematically accumulate in the positive direction as a consequence of absence of closure of the top part of the connection (the bottom part is generally closed throughout the tests). This connection behaviour also leads to a reduction of the pinching effects.

Imposed forces are shifted in the positive (hogging) direction for the innovative testing procedure whereas, apart from the asymmetry that may result from unsymmetrical connection detailing, positive and negative force amplitudes for ECCS tests are not excessively different.

The innovative testing procedure manages to capture the detrimental effects of the gravitational loads magnitude, that result in a reduction of available ductility as the magnitude of the gravitational loads increases, leading to premature collapse.

Failure of the connection is explicitly addressed by the innovative testing procedure since failure occurs when the connection is no longer able to withstand vertical load effects.

2.2.2.2 Beam 70 × 45 × 1.5

Figure 2.20 shows the hysteresis loops in terms of moment and rotation, for the cyclic tests performed on beam-to-upright connections specimens with beam 70 × 45 × 1.5 mm.

It can be observed that in the case of the tests performed according to the innovative cyclic testing procedure, the resulting imposed displacement history is unsymmetrical. In fact, displacements tend to systematically accumulate in the positive direction as a consequence of the absence of closure of the top part of the connection (the bottom part is generally closed throughout the tests). This connection behaviour also leads to a reduction of the pinching effects.

The response parameters for all cyclic tests are presented in Table 2.6 where, in addition to the elastic parameters (i.e. initial stiffness $S_{j,ini}$, yield moment M_y and rotation ϕ_y), the maximum positive (hogging) moment (M_u^+) and corresponding rotation (ϕ_u^+), as well as the minimum negative (sagging) moment (M_u^-) and corresponding rotation (ϕ_u^-) are reported, together with the number of cycles at failure N_c, the failure rotation ϕ_c and the bending moment for gravity loads (M_g).

The cyclic tests show practically the same initial stiffness of the monotonic tests (as shown in Fig. 2.21, in the case of an ECCS test). Strength deterioration can be observed in the cyclic test (70ECCS-1) for rotations larger than 40 mrad, in the case of sagging bending (top loading).

Strength is shifted in the positive (hogging) direction for the innovative testing procedure while, in the case of ECCS tests, the load carrying capacities under positive and negative bending are not excessively different, apart from the small asymmetry that may result from unsymmetrical connection detailing.

The innovative testing procedure allows a clear assessment of the detrimental effects of the magnitude of the gravitational loads that result in a reduction of available ductility as the magnitude of the gravitational loads increases, leading to premature collapse.

Figure 2.22 shows a re-analysis (in terms of Resistance, Absorbed energy and Rigidity ratios) of the cyclic test results carried out under different values of the gravity loads, while the typical observed failure modes are shown in Fig. 2.23.

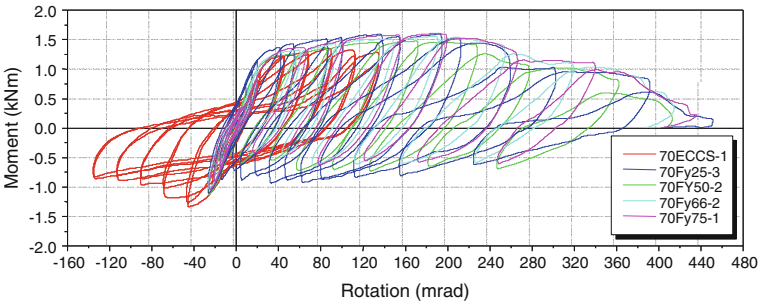

Fig. 2.20 Cyclic tests on beam 70 × 45 × 1.5 mm specimens

Table 2.6 Response parameters of the cyclic tests on beam 70 × 45 × 1.5 mm

Test	$S_{j,ini}$ [kNm/rad]	M_y [kNm]	ϕ_y [mrad]	M_u^+ [kNm]	ϕ_u^+ [mrad]	M_u^- [kNm]	ϕ_u^- [mrad]	N_c	ϕ_c [mrad]	M_g [kNm]
70ECCS-1	41.2	1.17	28.1	1.36	89.9	−1.34	−45.0	10	134.0	0.00
70ECCS-2	43.3	1.21	28.1	1.36	113.0	−1.40	−45.0	13	178.6	0.00
70Fy25-3	47.6	1.36	29.7	1.59	195.4	−0.94	65.0	11	393.1	0.30
70Fy25-4	47.7	1.22	26.0	1.55	191.2	−0.87	145.2	9	338.5	0.30
70Fy50-1	50.8	1.19	28.2	1.50	212.3	−0.81	125.1	8	427.6	0.60
70Fy50-2	50.9	1.17	28.2	1.48	197.4	−0.74	129.1	7	364.0	0.60
70Fy66-1	51.1	1.19	27.4	1.55	194.7	−0.61	74.6	6	331.5	0.79
70Fy66-2	43.8	1.20	26.4	1.57	193.0	−0.66	75.7	6	321.5	0.79
70Fy75-1	47.5	1.25	25.7	1.61	196.4	−0.64	81.7	6	342.0	0.90
Average All	**47.1**	**1.22**	**27.5**							
Average ECCS	**42.3**	**1.19**	**28.1**	**1.36**	**101.5**	**−1.37**	**−45**		**156.3**	
Average cyclic	**48.5**	**1.23**	**27.4**	**1.55**	**197.2**	**−0.75**	99.5		**359.7**	

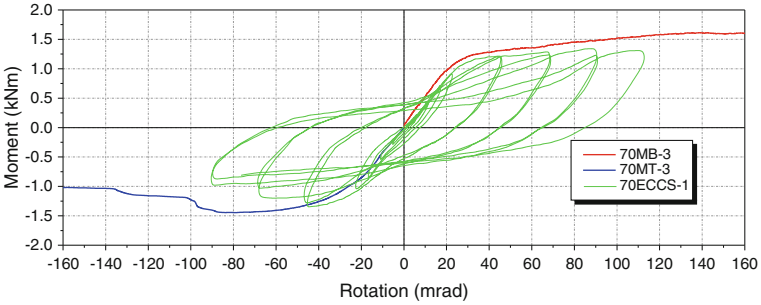

Fig. 2.21 Comparisons of the ECCS cyclic and monotonic tests for 70 × 45 × 1.5 mm beam specimen

In the case of ECCS cyclic testing procedure, the degradation of resistance and stiffness of the connection under hogging bending were lower than in sagging bending.

In the case of tests performed according to the innovative procedure, the amplitude of the displacements in the post-elastic phase (depending on different values of gravitational force F_g) did not change significantly the resistance, stiffness and ductility of the connection. According to the previous definitions (Fig. 2.17), connection 70Fy50-2 exhibited type I failure mode, while all other (70 × 45 × 1.5 mm beam) specimens exhibited failure mode type II.

Premature collapse occurred as the magnitude of the gravity loads increased.

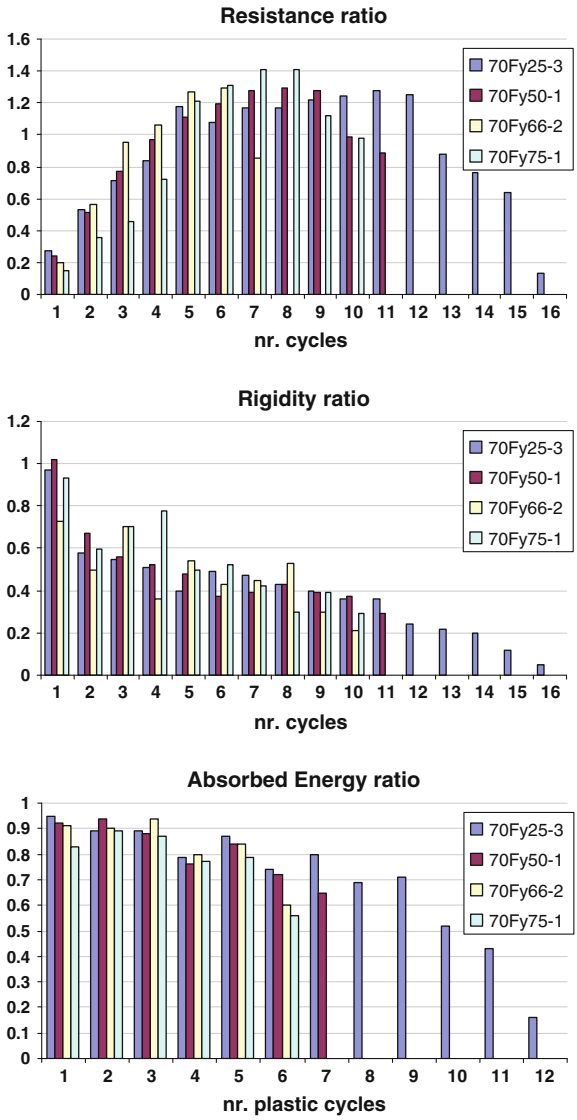

Fig. 2.22 Cyclic tests on 70 × 45 × 1.5 mm beam specimens

In all cyclic tests, the observed collapse mechanisms observed were the same as in monotonic tests under hogging bending, but with amplified deformations. At the end of some tests with a gravitational force of 50, 66 and 75 % of the yield strength, fracture of the beam end-plate connector occurred around the upper hole (Fig. 2.23).

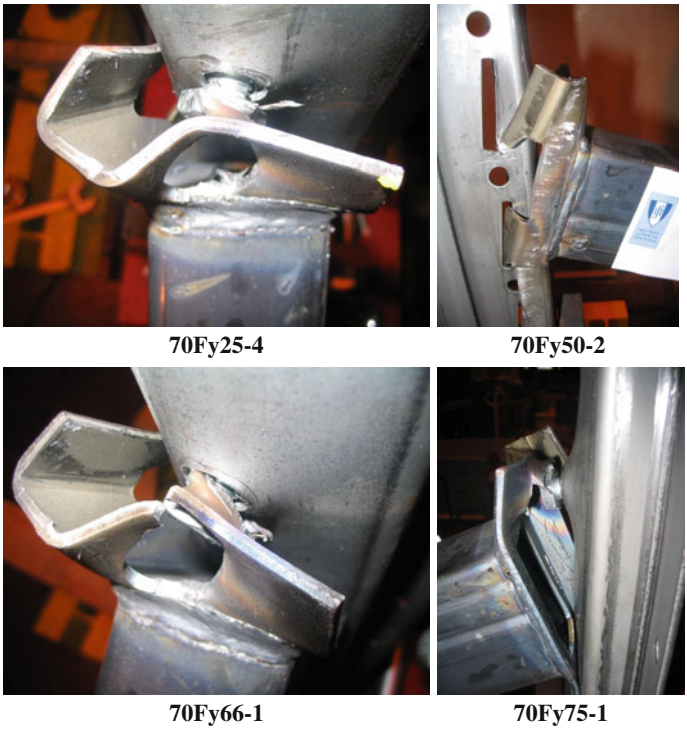

Fig. 2.23 Cyclic tests on 70 × 45 × 1.5 mm beam specimens—failure modes

2.2.2.3 Beam 130 × 45 × 1.5

Figure 2.24 shows the hysteresis loops in terms of moment and rotation, for the cyclic tests performed on beam-to-upright connections specimens with beam 130 × 45 × 1.5 mm.

The response parameters for all cyclic tests with a beam 130 × 45 × 1.5 mm are presented in Table 2.7, with the same symbols used (and described) in Table 2.6.

As shown in Fig. 2.24, the number of cycles to failure is strongly influenced by the intensity of the vertical (gravity) load.

The cyclic tests show practically the same initial stiffness when compared to the monotonic tests (as shown in Fig. 2.25, in the case of an ECCS test). The degradation levels of the resistance during the cyclic test (130ECCS-3) were nearly the same for both ways of loading (hogging and sagging bending).

Figure 2.26 shows a comparison (in terms of Resistance, Absorbed energy and Rigidity ratios) of the cyclic test results carried out under different values of the gravity loads.

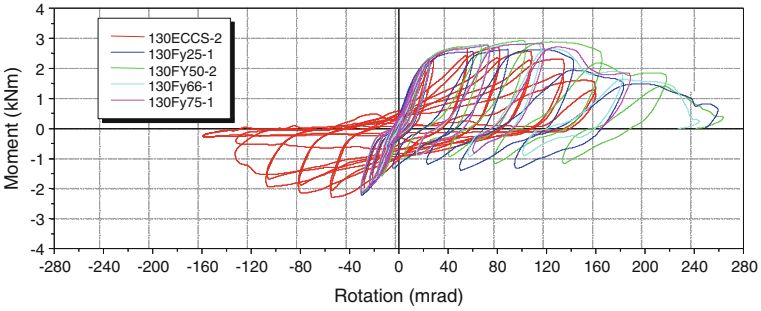

Fig. 2.24 Cyclic tests on beam 130 × 45 × 1.5 mm specimens

In the case of ECCS cyclic testing procedure, the resistance and stiffness ratios of the connection under hogging bending (bottom loading) were higher than under sagging bending (top loading).

In the case of tests performed according to the innovative procedure, a gradual deterioration of the energy dissipation capacity was observed. The resistance rate was satisfactory until the sixth cycle, after which a reduction occurred.

Despite of the high degradation of stiffness in the third cycle for the model 130Fy75-1, the ratio remained stable throughout the subsequent part of the test. In the other specimens, the stiffness degradation was satisfactory since no sudden decrease from one cycle to another occurred.

Figure 2.27 shows some images of the collapse mechanisms during the cyclic tests.

Premature collapse as well as reduction of the rotation capacity was observed as the magnitude of the gravity loads increased. At the end of the test the beam end connector was connected to the upright only by means of the bolt which sometimes could punch through the end-plate (Fig. 2.27).

According to the previous definitions (Fig. 2.17), the collapse mode for the connections 130Fy25-1 and 130Fy75-1 was type I while for 130Fy50-2 and 130Fy66-1 was type II.

2.2.3 Comparison and Analysis of Test Results

2.2.3.1 Monotonic Tests

Effect of the beam size on the main parameters (yield and ultimate strength, initial stiffness, yield and ultimate rotation) is shown in Table 2.8, with reference to monotonic tests.

Figure 2.28 shows the comparison between the moment—rotation curves for both beam sizes, and loading conditions.

Table 2.7 Response parameters of the cyclic tests for beam 130 × 45 × 1.5 mm

Test	$S_{j,ini}$ [kNm/rad]	M_y [kNm]	ϕ_y [mrad]	M_u^+ [kNm]	ϕ_u^+ [mrad]	M_u^- [kNm]	ϕ_u^- [mrad]	N_c	ϕ_c [mrad]	M_g [kNm]
130ECCS-2	85.0	2.51	25.9	2.70	79.3	−2.30	−53.2	10	157.5	0.00
130ECCS-3	104.3	2.47	22.2	2.80	79.5	−2.23	−52.9	9	157.5	0.00
130Fy25-1	107.2	2.38	25.5	2.64	117.9	−1.39	52.6	5	259.6	0.63
130Fy25-2	80.1	2.51	24.5	2.83	123.1	−1.27	49.5	4	175.6	0.63
130Fy50-1	115.4	2.62	29.6	2.97	130.9	−1.13	74.0	4	210.8	1.26
130Fy50-2	95.3	2.54	28.3	2.89	126.2	−1.19	136.4	4	218.3	1.26
130Fy66-1	84.8	2.46	23.1	2.84	116.1	−0.95	103	3	182.8	1.66
130Fy66-2	92.2	2.40	22.8	2.73	111.7	−1.19	136.4	3	182.8	1.66
130Fy75-1	107.0	2.47	24.2	2.83	118.7	−0.87	63	2	118.3	1.89
Average All	**96.8**	**2.48**	**25.1**							
Average ECCS	**94.7**	**2.49**	**24.05**	**2.75**	**79.4**	**−2.27**	**−53.1**		**157.5**	
Average cyclic	**97.4**	**2.48**	**25.4**	**2.82**	**120.7**	**−1.14**	**87.8**		**192.6**	

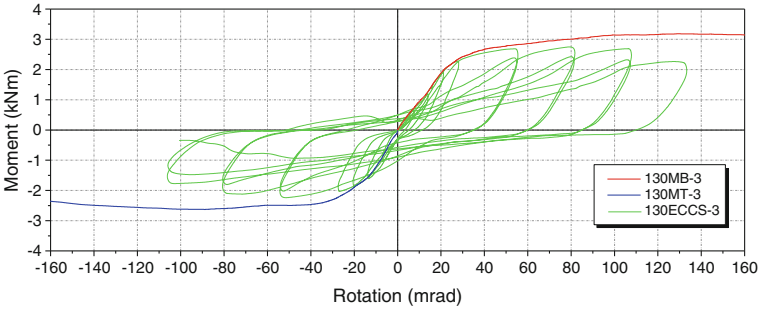

Fig. 2.25 Comparisons of the cyclic and monotonic tests for 130 × 45 × 1.5 mm beam

Fig. 2.26 Cyclic tests on 130 × 45 × 1.5 mm beam specimens

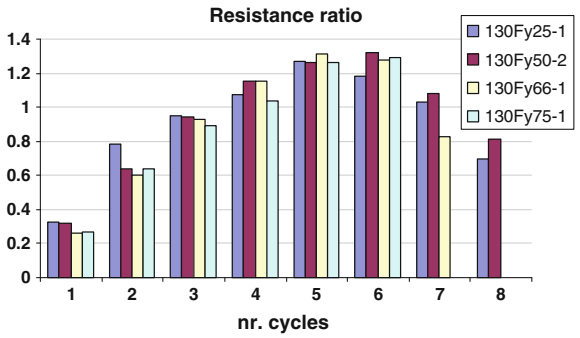

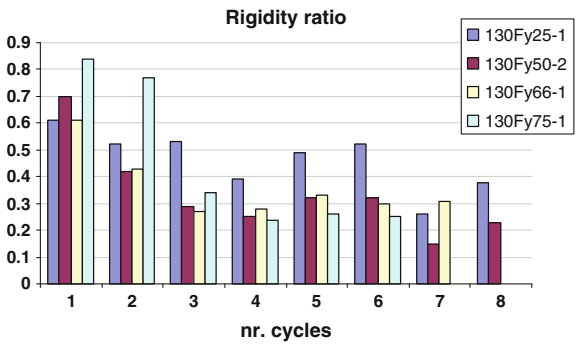

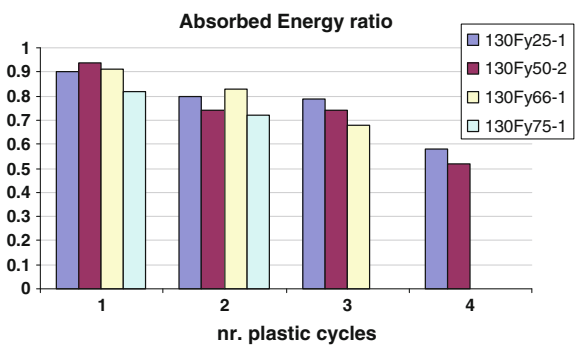

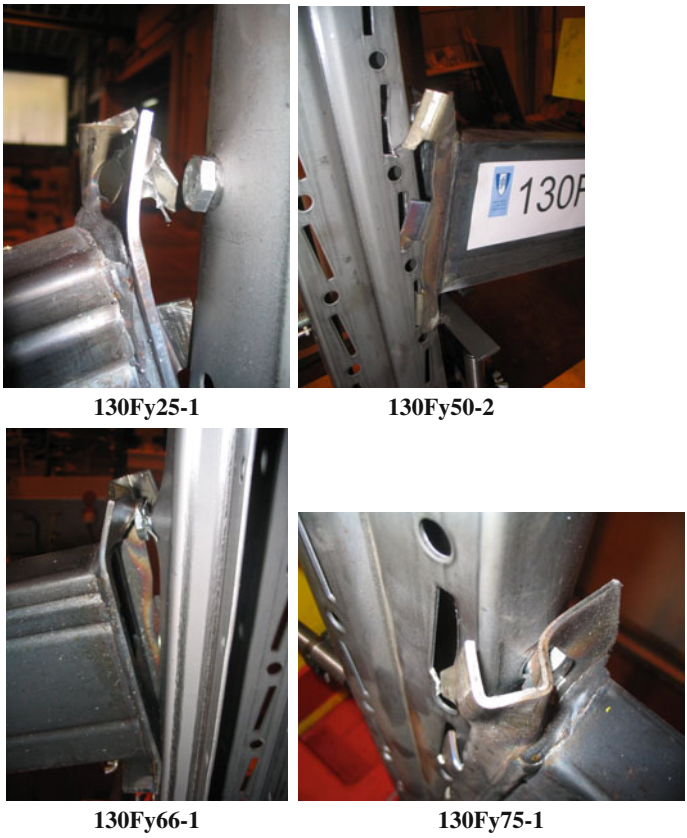

Fig. 2.27 Cyclic tests on 130 × 45 × 1.5 mm beam specimens—failure modes

Examining Table 2.8 and Fig. 2.28 it can be noticed that connections with 130 × 45 × 1.5 mm beam showed larger stiffness than those with 70 × 45 × 1.5 mm beam.

Furthermore, stiffness of the connections with 130 × 45 × 1.5 mm beams under sagging bending is approximately 25 % larger than that under hogging bending, because of the different collapse mechanisms, shown in Figs. 2.13 and 2.14. Under hogging bending (Figs. 2.13 and 2.29c), the safety bolt is in tension, and only one hook (that finally comes out from the hole in the upright) participates to the resistant mechanism, together with the end-plate in bending. Collapse mechanism, in this case, is due to deformation of the end-plate, to punching of the safety bolt through the end-plate and to deformation of one hook (a second one is only partially deformed). Under sagging bending (Figs. 2.14 and 2.29b), on the contrary, two hooks participate to the resistant mechanism, while the safety bolt doesn't, because it is in the compression zone. This differences explain both the higher stiffness and the smaller yield strength and rotation (as well as ultimate strength and rotation)

Table 2.8 Effect of the beam size—monotonic tests

Loading	Beam	M_y [kNm]	ϕ_y [mrad]	$S_{j,ini}$ [kNm/rad]	M_u [kNm]	ϕ_u [mrad]
Hogging bending	130 × 45 × 1.5	2.53	26.0	95.8	3.14	129.7
	70 × 45 × 1.5	1.23	27.8	47.9	1.60	178.7
Ratio	**130/70**	**2.06**	**0.94**	**2.00**	**1.96**	**0.73**
Sagging bending	130 × 45 × 1.5	2.11	18.8	119.0	2.44	107.3
	70 × 45 × 1.5	1.24	26.0	48.9	1.42	77.7
Ratio	**130/70**	**1.70**	**0.72**	**2.43**	**1.72**	**1.38**

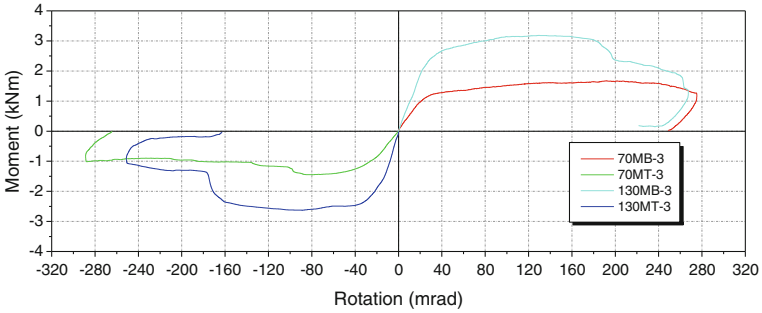

Fig. 2.28 Monotonic moment—rotation curves for both beam sizes and loading directions

exhibited by the 130 × 45 × 1.5 mm beam-to-upright connection under sagging bending with respect to the same connection under hogging bending.

The non symmetric geometry (and stiffness) of the end plate would cause a rotation of the beam in the horizontal plane (as shown in Fig. 2.29b). Such a rotation is however prevented by the test set up. Hence, all deformation concentrates in the end-plate connector and in the hooks.

The elastic behaviour of the 70 × 45 × 1.5 mm. beam-to-upright connection was practically symmetric, under hogging and sagging bending, as shown in Table 2.8. On the contrary, the ultimate behaviour of this connection under sagging bending was very different from the one exhibited under hogging bending, as evidenced in the same table, as well as in Figs. 2.10 and 2.11.

Under hogging bending, the safety bolt is in tension, and the center of rotation is located at the lower flange of the beam (in compression) as sketched in Fig. 2.29c. The end plate is extended, below the lower flange of the beam, in order to allow presence of a third hook. As evidenced in Fig. 2.10, the central hook is located approximately in correspondence of the lower flange of the 70 × 45 × 1.5 mm beam (i.e. at the center of rotation), so it doesn't participate to the resistant mechanism. Collapse mechanism, in this case, is due to deformation of the end-plate, punching

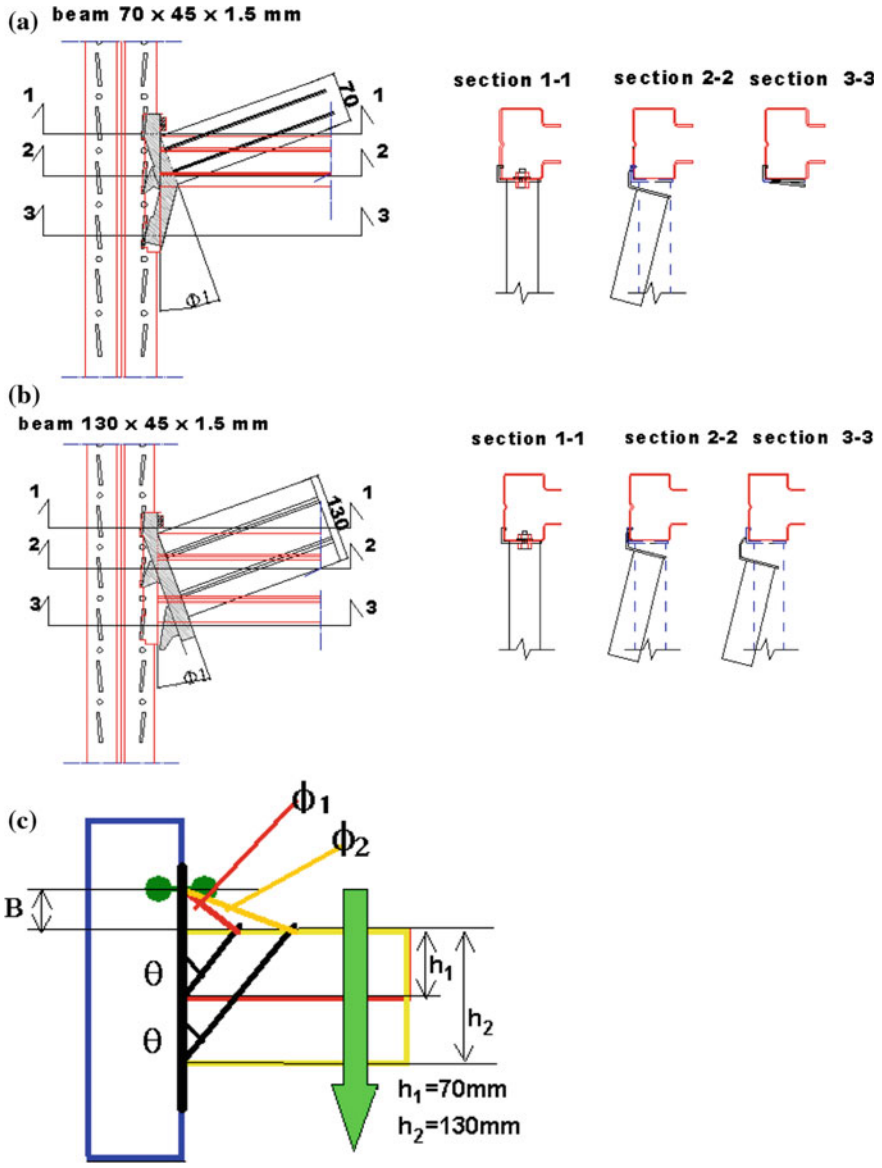

Fig. 2.29 Schematic of the connection kinematics and failure mechanisms

of the safety bolt through the end-plate and to deformation of one hook (the upper one, which can be seen as partially deformed in Fig. 2.10).

Under sagging bending (Fig. 2.11), on the contrary, the center of rotation is close to the upper flange of the beam, while the safety bolt is in the compression zone. The portion of the end-plate, extended below the lower flange, is restrained, on one

side, by the lowest hook. Furthermore, the whole end-plate is stiffened on the "hooked" side, by the presence of the edge stiffener represented by the bent portion of the L shaped plate. When the beam is bent upward, the deformation of the lower part of the end plate, should comply with the restraints represented by the lower flange of the beam, by the lowest hook and by the stiffened edge. Its deformed shape is hence the one shown in Fig. 2.11 and sketched in Fig. 2.29a. The presence of the hooks and of the stiffened edge, forces the end-plate to bend in both the vertical and the horizontal plane. Accordingly should do the beam, which is however restrained to out-of-plane bending by the test set-up (as shown in Fig. 2.6).

This results in a concentration of deformations at the fillet weld connecting the beam to the end plate, on the side of the stiffened (hooked) edge, that fractures with consequent collapse of the connection (Fig. 2.11). Crack initiates at the end of the vertical leg of the fillet weld connecting the beam to the end-plate. This is the most stressed point of the connection, also because of the stress concentration due to the fact that the beam is fillet welded to the end plate on three sides only, and the fillet is not returned around the corner, despite of what is recommended by clause 4.3.2.1 (4) of EN 1993-1-8:2005 (*"Fillet welds finishing at the ends or sides of parts should be returned continuously, full size, around the corner for a distance of at least twice the leg length of the weld, unless access or the configuration of the joint renders this impracticable."*).

Figure 2.30 show a classification of both the connections, according to Eurocode 3 (2005)—Part 1.8, adopting respectively the length of the beam L_b = 1.8 m, as for the structures tested full scale within this research, and L_b = 2.7 m, as in the most common real applications of racks where, at each level and for each span, up to three pallets can be placed side-by-side on a couple of beams.

In Fig. 2.30, according to Eurocode 3 (2005)—Part 1.8, $m = M/M_{y,b}$ and $\phi = \phi/\phi_{y,b}$, where M and ϕ are the actual moment and rotation experimentally measured, and $M_{y,b}$ and $\phi_{y,b}$ are the conventional yield moment and rotation of the beam. $M_{y,b} = f_y * W_b$ is the product of the yield stress of the material (f_y) times the section modulus (W_b) of the beam cross section, while $\phi_{y,b} = M_{y,b}/k_b$ is the ratio of $M_{y,b}$ (previously defined) to the beam conventional elastic stiffness $k_b = (EI_b)/L_b$, I_b being the moment of inertia of the beam and E the Young's Modulus.

It can be noticed that for a beam length of 1800 mm (Fig. 2.30a) the connection with beam 70 × 45 × 1.5 can be considered as semi-rigid while in the case of beam 130 × 45 × 1.5, the same end-plate connection behaves as flexible. When the beam length is increased to 2700 mm (Fig. 2.30b), both connections can be considered semi-rigid.

2.2.3.2 Cyclic Tests

The effect of the beam size and of the gravity loads in terms of hysteresis loops, is shown in Figs. 2.31 and 2.32, respectively with reference to ECCS and to cyclic tests, as well as in Table 2.9 that summarizes the mean values of the response

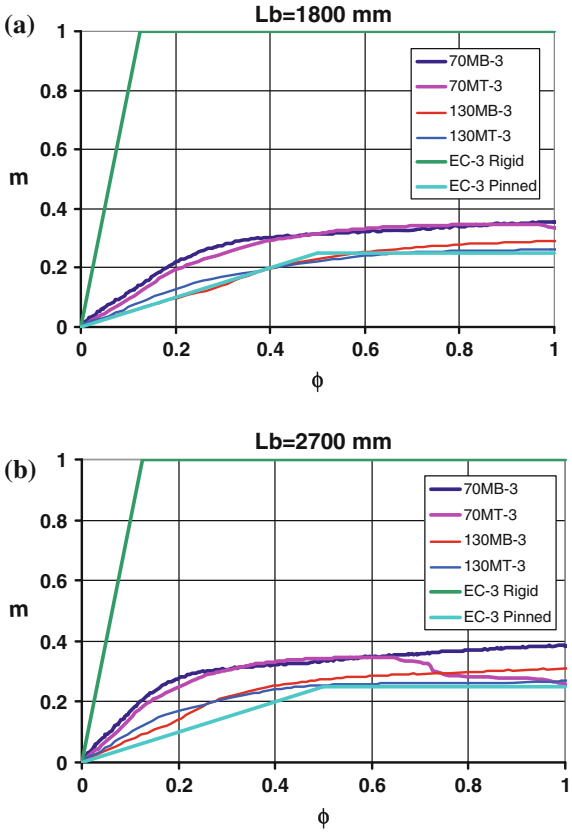

Fig. 2.30 Classification of the beam-to-upright connections according to EN 1993-1-8:2005

parameters for both 70 × 45 × 1.5 mm (a) and 130 × 45 × 1.5 mm (b) beam, and for different values of the gravity loads.

In Table 2.9, in addition to the elastic parameters (i.e. initial stiffness $S_{j,ini}$, yield moment M_y and rotation ϕ_y), the maximum positive (hogging) moment (M_u^+) and corresponding rotation (ϕ_u^+), as well as the minimum negative (sagging) moment (M_u^-) and corresponding rotation (ϕ_u^-) are reported together with the number of cycles at failure N_c, the failure rotation ϕ_c and the bending moment for gravity loads (M_g). It is evident that the response of the connections under symmetric cycles and in absence of gravity loads (ECCS tests, Fig. 2.31) is very different from that of the same connections tested in presence of gravity loads (Fig. 2.32).

In particular, the response of the specimens tested in presence of gravity loads is characterized by cyclic creep (ratcheting), with a progressive accumulation of plastic deformation in the same direction of the mean applied load. The measured ratcheting rate increases with the applied gravity load.

Collapse of the connection is attained approximately under the same rotation ϕ_c (360 mrad for 70 × 45 × 1.5 mm beams and 192 mrad for 130 × 45 × 1.5 mm beams), although some dependence of ϕ_c on the applied gravity load can be

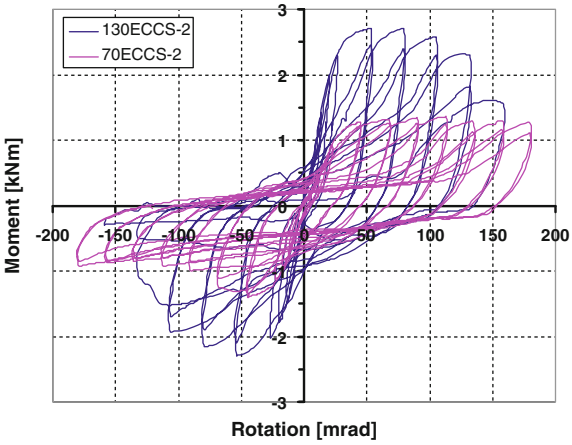

Fig. 2.31 Effect of the beam size—ECCS cyclic tests

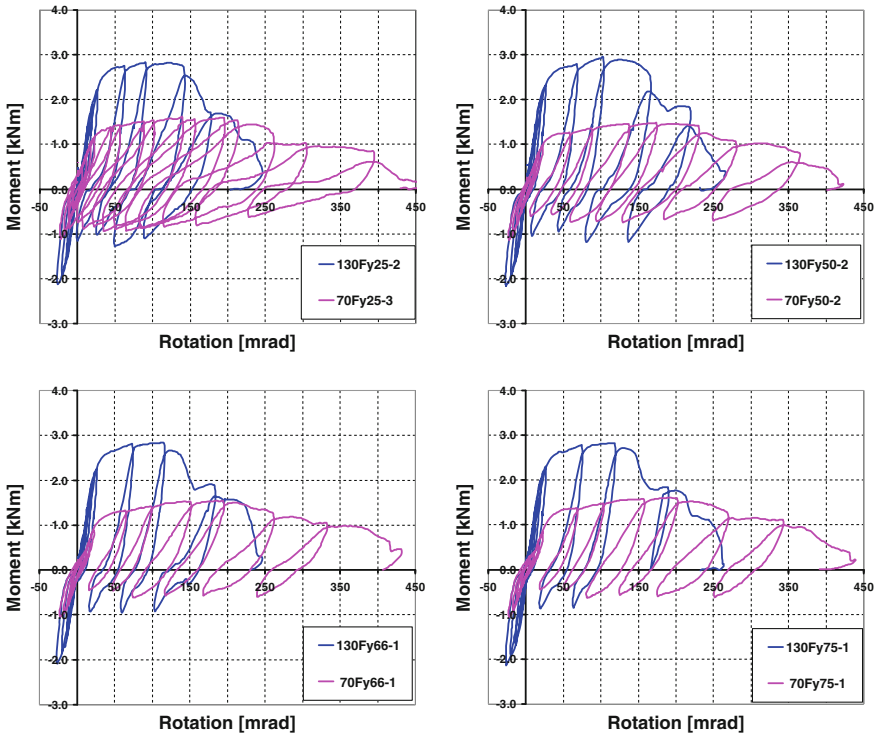

Fig. 2.32 Effect of the beam size and of the gravity loads—cyclic tests

Table 2.9 Average values of response parameters for 70 × 45 × 1.5 mm (a) and 130 × 45 × 1.5 mm (b) beams

	M_g [kNm]	$S_{j,ini}$ [kNm/rad]	M_y [kNm]	ϕ_y [mrad]	M_u^+ [kNm]	ϕ_u^+ [mrad]	M_u^- [kNm]	ϕ_u^- [mrad]	N_c	ϕ_c [mrad]
(a)										
70-ECCS	0.00	42.25	1.19	28.10	1.36	101.45	−1.37	−45.00	11.5	156.30
70-Fy25	0.30	47.65	1.29	27.85	1.57	193.30	−0.91	105.10	10	365.80
70-Fy50	0.60	50.85	1.18	28.20	1.49	204.85	−0.78	127.10	7.5	395.80
70-Fy66	0.79	47.45	1.20	26.90	1.56	193.85	−0.64	75.15	6	326.50
70-Fy75	0.90	47.50	1.25	25.70	1.61	196.40	−0.64	81.70	6	342.00
(b)										
130-ECCS	0.00	94.65	2.49	24.05	2.75	79.40	−2.27	−53.05	9.5	157.50
130-Fy25	0.63	93.65	2.45	25.00	2.74	120.50	−1.33	51.05	4.5	217.60
130-Fy50	1.26	105.35	2.58	28.95	2.93	128.55	−1.16	105.20	4	214.55
130-Fy66	1.66	88.50	2.43	22.95	2.79	113.90	−1.07	119.70	3	182.80
130-Fy75	1.89	107.00	2.47	24.20	2.83	118.70	−0.87	63.00	2	118.30

observed, at least for large values of the gravity load (66 and 75 % of the yield load). Hence, connections of beams supporting a high gravity load collapse at a number of cycles (N_c) smaller than those supporting a smaller gravity load, due to the different creep rate.

Hysteresis loops are clearly non symmetric, with similar maximum values of the hogging moment (M_u^+) and of its corresponding rotation (ϕ_u^+), practically independent on the applied gravity load, but with the minimum values of the sagging moment (M_u^-) and of its corresponding rotation (ϕ_u^-) becoming (in absolute value) smaller and smaller when increasing the gravity load. Of course, the elastic parameters (i.e. initial stiffness $S_{j,ini}$, yield moment M_y and rotation ϕ_y) are not influenced by the value of the applied gravity load, as shown in Fig. 2.33.

Dependence of the various inelastic response parameters on the applied gravity load (M_g) is shown in Fig. 2.34.

In absence of gravity load (ECCS tests), the response of the specimens is nearly symmetric; little non symmetry is due to the different response of the connection under hogging and sagging bending, already highlighted in the case of monotonic tests. In particular, it should be noticed that under sagging bending the connections show a lower ductility than under hogging bending ($\phi_u^- < \phi_u^+$). The values of M_u^+, ϕ_u^+, M_u^- and ϕ_u^- (Table 2.9) are (in absolute value) smaller than those measured in monotonic tests (reported in Table 2.8), because obtained under cyclic loading.

Differences can also be noticed in the failure modes of the different specimens.

In absence of gravity loads (ECCS tests), failure occurred always under sagging bending, i.e. under the loading condition for which the connection showed the

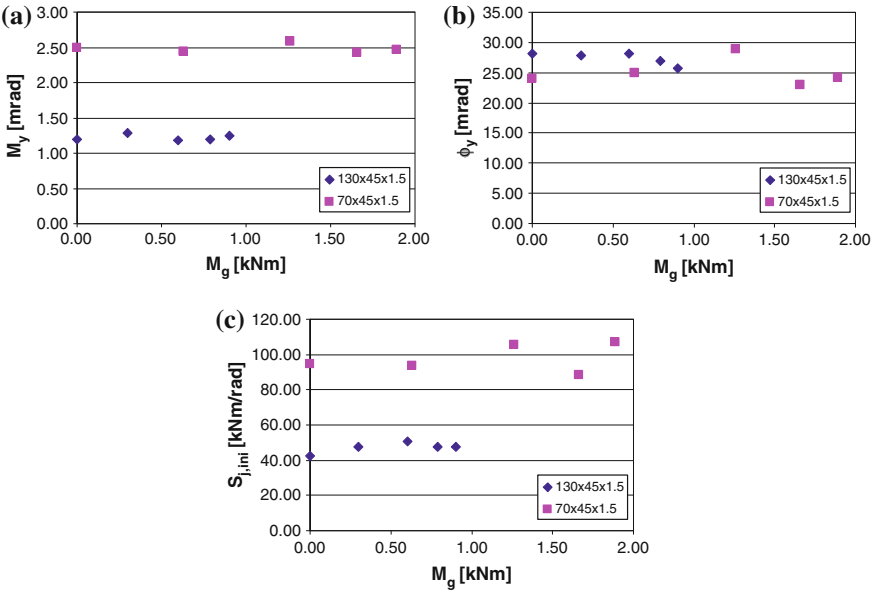

Fig. 2.33 Comparison of elastic response parameters for ECCS and cyclic tests

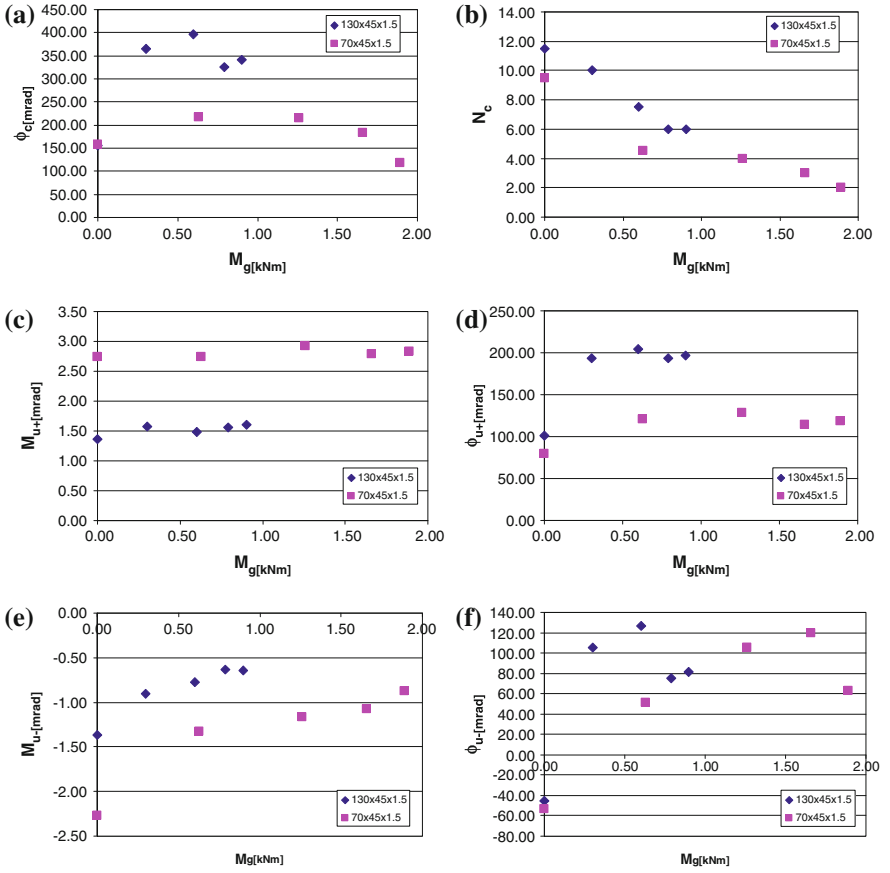

Fig. 2.34 Comparison of ultimate response parameters for ECCS and cyclic tests

lower strength and ductility in monotonic tests. In the case of 70 × 45 × 1.5 mm beams the collapse mechanism involved cracking of the fillet weld connecting the beam to the end-plate, deformation of the end plate and of the central hook and a small deformation of the lowest hook. In this case, however, due to the cyclic load reversals, deformation of the upper hook as well as partial punching of the safety bolt through the end-plate could be observed. Also in the case of 130 × 45 × 1.5 mm beams, the collapse mechanism for cyclic (ECCS) tests is similar to the one described for monotonic tests under sagging bending, with deformation of the two lowest hooks. Furthermore, also in this case, due to the cyclic load reversals, large deformation of the upper hook as well as partial punching of the safety bolt through the end-plate could be observed. In presence of gravity loads, on the contrary, failure occurred always under hogging bending. No difference could be noticed in the failure mechanisms under increasing values of the gravity loads, but only a smaller number of cycles to failure. Collapse mechanism,

for both 70 × 45 × 1.5 mm and 130 × 45 × 1.5 mm beams, involved complete punching of the safety bolt through the end-plate, with partial deformation of the central and of the lowest hooks, because of the cyclic reversal loading. Cracking of the hooks was also observed.

2.2.4 Conclusions

- The failure mode for 70 mm (hogging bending) and 130 mm (hogging and sagging bending) deep beams consisted of large deformations in the top zone of the beam end connector.
- In the 70 mm deep beam subject to sagging bending, the failure mode was the fracture of the fillet weld between the beam and the end-plate connector.
- The connection behaviour for all tests was not influenced by safety bolt deformation, whose axial stiffness is much larger than the bending stiffness of the end-plate connector.
- The rotation capacity difference between the loading directions was larger for the 70 mm deep beam due to different collapse occurred in the sagging loading.
- According to Eurocode 3 (2005) the connection with a 70 mm deep beam can be considered as semi-rigid, for both beam lengths of 1.8 and 2.7 m.
- According to Eurocode 3 (2005) the connection with a 130 mm deep beam can be considered as semi-rigid for a beam lengths of 2.7 m, and as flexible for a beam lengths of 1.8 m (as in the case of the structures tested full scale within this research); hence, in this last case, the influence of the connection behaviour may be ignored in structural analysis.
- The results of test performed with the innovative cyclic testing procedure were fundamentally different from those obtained through the application of the ECCS recommended testing procedure.
- In the tests performed according to the innovative cyclic testing procedure, the imposed displacement history is unsymmetrical. Displacements tend to systematically accumulate in the positive direction as a consequence of the absence of closure of the top part of the connection (the bottom part is generally closed throughout the tests). This connection behaviour also leads to a reduction of the pinching effects.
- In the innovative testing procedures, the imposed forces are shifted in the positive (hogging) direction whereas, apart from the asymmetry that may result from unsymmetrical connection detailing, positive and negative force amplitudes for ECCS tests are not excessively different.
- Failure of the connection is explicitly addressed by the innovative testing procedure since failure occurs when the connection is no longer able to withstand vertical load effects.

2.3 Column Base Connections

Proprietary moment connections are typically used as column-base connections for steel selective pallet storage racks. This study focuses on the base connection type shown in Fig. 2.35.

The column bases consist of two vertical steel gusset plates fillet-welded to the base plate. The upright is connected to the base by bolting through the slotted holes in the gusset plates using two M10 × 25 (grade 8.8) bolts for each vertical plate.

The base plate is connected to the foundation surface (in this case either in concrete or in steel) by means of two M16 (grade 8.8) bolts. All bolts are preloaded.

As a general remark, it should be noticed that this proprietary column-base connection is strongly non-symmetric in cross-aisle direction, where an eccentricity of 66.5 mm exists between the bolt line and the c.o.g. of the up-right profile.

A non-symmetric response is hence to be expected in cross-aisle direction under transverse load reversals, when the bolts may be either in tension or in compression.

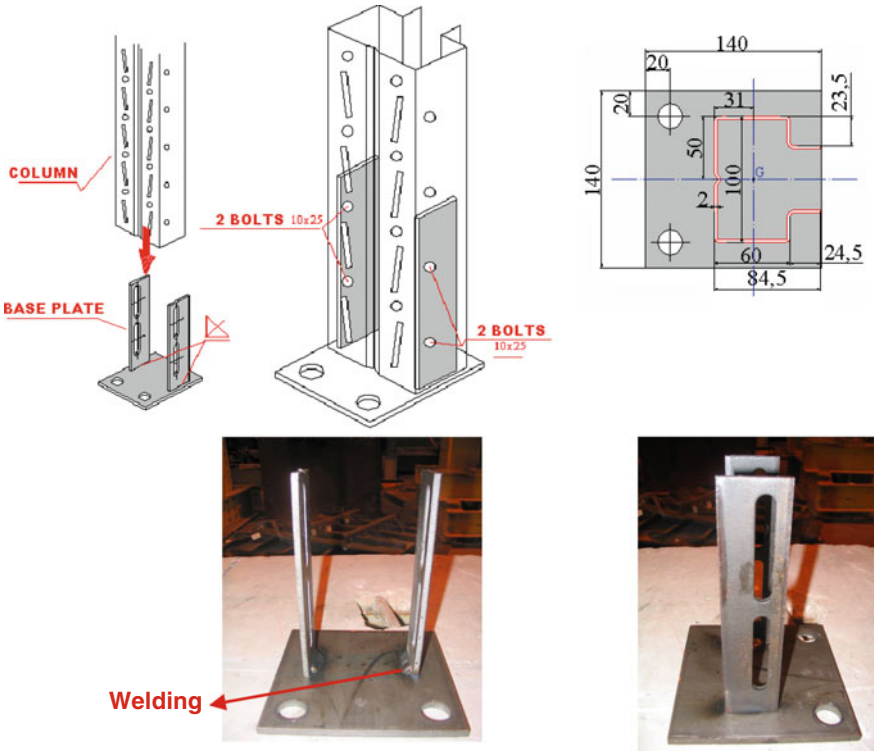

Fig. 2.35 Details of base plate and base-to-upright connections

Objectives of the tests on column base connections were:

- Assessment of the moment-rotation curves
- Assessment of the collapse modes

under either monotonic or cyclic transversal loads, for different levels of axial load applied to the upright.

The specimens were tested in the cross-aisle and down-aisle directions. In the cross-aisle direction the specimens were subjected to a monotonic load in two different directions, in order to allow respectively tension and compression in the anchor bolts of the column base connection.

One type of upright cross-section (100/20b), whose geometrical properties are shown in Table 2.10 was studied under four values of axial load: 0, 25, 50 and 75 kN. These correspond respectively to 0, 17, 34 and 52 % of the yield resistance of the net cross section under axial load (Af_y), f_y being the nominal yield strength of 275 MPa.

Column bases connected to steel and concrete surfaces were examined.

In the full scale dynamic tests carried out at NTUA the base plates were welded to the steel deck of the shaking table; hence some tests were carried out with the steel base welded and bolted to a steel surface. These tests are indicated hereafter as "Athens base" tests.

Table 2.11 summarizes the performed tests. The size and shape of the test specimen are shown in Fig. 2.36, while the test set up and instrumentation are shown in Figs. 2.37 and 2.38.

The tested specimens comprise a portion of upright 100/20b, 650 mm long, connected to a special steel plate at the top and to the ordinary base plate at the bottom. The steel plate at the top, welded to the upright, allowed the coupling of the specimen to the actuator, by means of four M16 (grade 8.8) preloaded bolts.

The specimens were tested in a system composed by a main reaction frame, a mechanical actuator and a secondary frame used to induce the axial force in the specimens.

In order to simulate different "floor conditions", the specimens were connected either to a steel member or to a concrete block. These, in turn, where connected to the main frame using bolts. The lateral displacements at the top of the specimens

Table 2.10 Geometrical properties of the upright 100/20b

Properties	Gross section	Net section
A [mm^2]	588.8	525.7
t [mm]	2.0	2.0
J_x [mm^4]	436020	406100
J_y [mm^4]	812280	694680
W_x [mm^3]	8543	8330
W_y [mm^3]	16747	14323

Table 2.11 Column-base tests

Type	Test	Steel base (bolted)			Athens base (bolted & welded)
		No axial load	Axial load 25 kN	Axial load 50 kN	Axial load 25 kN
(a)					
	Monotonic	SBCB-1 SBCB-2 SBCB-3 SBCB-4 SBCB-5	SBCBF25-1 SBCBF25-2	SBCBF50-1 SBCBF50-2	ASBCBF25-1
	Monotonic	SBCT-1 SBCT-2 SBCT-3 SBCT-4 SBCT-5	SBCTF25-1 SBCTF25-2	SBCTF50-1 SBCTF50-2	ASBCTF25-1
	Monotonic	SBDB-1 SBDB-2 SBDB-3 SBDB-4 SBDB-5	SBDBF25-1 SBDBF25-2 SBDBF25-3	SBDBF50-1 SBDBF50-2	ASBDBF25-1
	Cyclic	———–	SBCCF25-1	————	ASBCCF25-1
	Cyclic	———–	SBDCF25-1	————	ASBDCF25-1
Type	Test	Concrete base—Hilti			
		No axial load	Axial load 25 kN	Axial load 50 kN	Axial load 75 kN
(b)					
	Monotonic		CBCBF25-1 CBCBF25-2	CBCBF50-1 CBCBF50-2	CBCBF75-1
	Monotonic		CBCTF25-1	CBCTF50-1	CBCTF75-1
	Monotonic	CBDB-1	CBDBF25-1 CBDBF25-2	CBDBF50-1 CBDBF50-2 CBDBF50-3	CBDBF75-1
	Cyclic		CBCCF25-1	CBCCF50-1	CBCCF75-1
	Cyclic		CBDCF25-1	CBDCF50-1	CBDCF75-1

Connected to (a) a steel surface, (b) a concrete surface

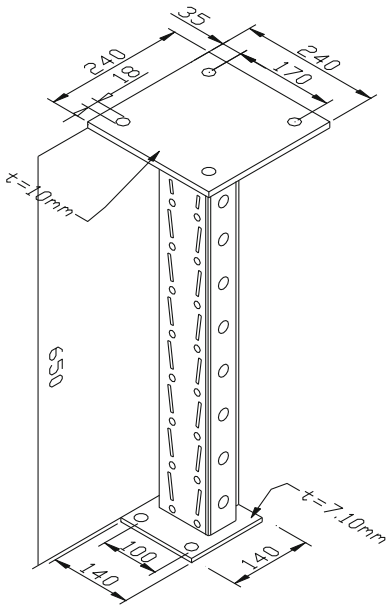

Fig. 2.36 Specimen shape and size

were restrained using double angles welded to a metallic member that was connected to the main frame, as shown in Fig. 2.37.

The axial force was imposed in the centre of gravity of the upright using two 36 mm Dywidag bars. The system of application of the axial force comprised a secondary reaction frame, a beam, two hydraulic actuators and two loading cells, as shown in Fig. 2.38.

The Dywidag bars, 8 m long, were connected to the head of the actuator, which was bolted to the plate at the top of the upright.

Tests were carried out under displacement controlled conditions. The actuator applied the transversal displacement at a distance of 1 m from the column base, while the imposed load was measured through a load cell. Four electric displacement transducers (LVDTs) were positioned in the column base to evaluate the relative bending of the base, as shown in Fig. 2.37.

The moment-rotation curves were plotted for each test; the moment at the column base is $M = F * a$ and the rotation of the connection is evaluated according to Eq. 2.2.

$$\phi = \frac{V}{a} \tag{2.2}$$

where V is the displacement imposed at the top of the specimen by the transversal load F applied with a lever arm a = 1.0 m with respect to the specimen base.

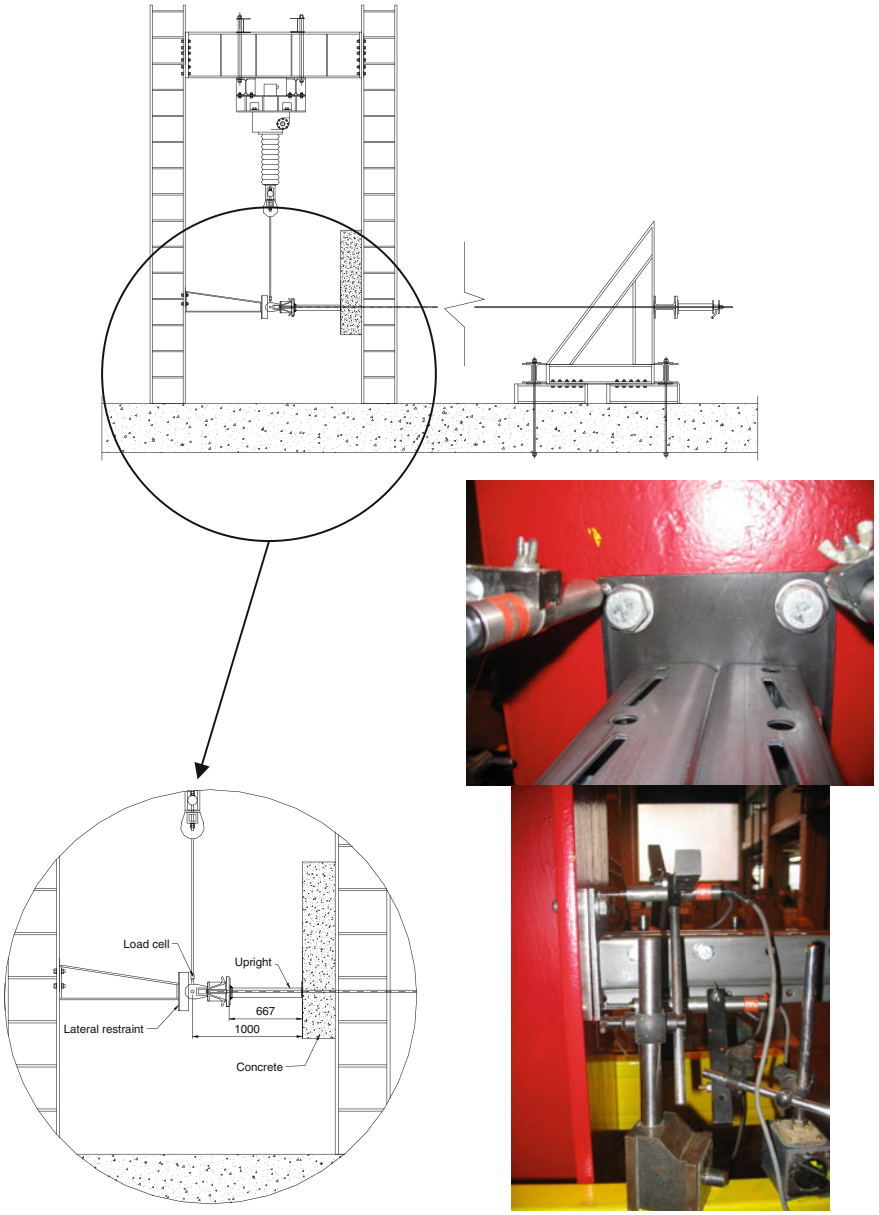

Fig. 2.37 Test set-up and instrumentation

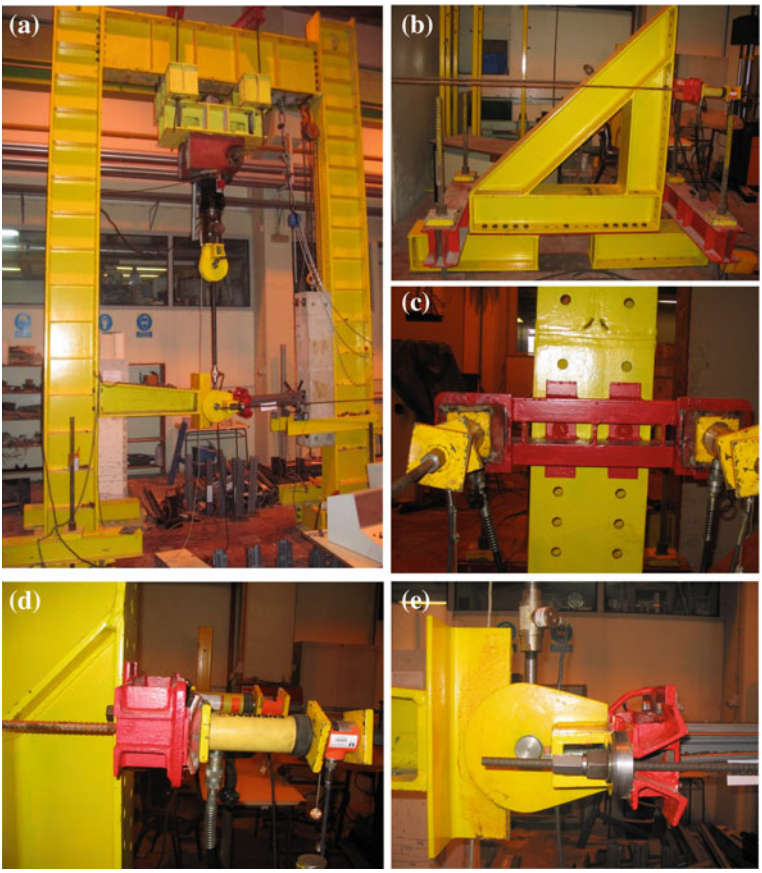

Fig. 2.38 Test set-up: **a** main frame, **b** secondary reaction frame, **c** axial load system connected to the secondary reaction frame, **d** details of jacks and Dywidag bars connected to the secondary reaction frame, **e** details of Dywidag bars, their connection to the head of the actuator, as well as of the lateral displacements restraint

2.3.1 Monotonic Tests

2.3.1.1 Cross-Aisle

2.3.1.1.1 Bolts in Tension

Table 2.12 summarizes the results of monotonic tests carried out in cross-aisle direction on column-base connections, with anchor bolts in tension. Different values of the axial load were considered (0, 25, 50 and 75 kN). Different types of connection of the upright steel base to the floor were also considered: bolted to a steel or to a concrete floor, as well as bolted-and-welded to a steel deck (as in the

Athens dynamic shaking table tests). Table 2.12 summarizes, for the different types of connections, and for each test, the yield bending moment M_y and rotation ϕ_y, the initial elastic stiffness $S_{j,ini}$, the maximum bending moment M_{max} and associated rotation ϕ_{max}, the energy absorbed up to the attainment of the maximum rotation ϕ_{max}, as well as the failure mode exhibited by the specimen.

Repetitions were carried out under similar testing conditions, in order to verify the reliability of the results.

In some cases, test repetition resulted in different failure modes. For this reason, Table 2.12 report the average values of tests carried out under similar conditions, as well as the average values for those tests, performed under similar conditions, but characterized by the same failure mode.

Figures 2.39 and 2.40 show a comparison of the moment-rotation curves for column-base connections with anchor bolts in tension, under different values of the axial load, connected respectively to a steel deck (Fig. 2.39) and to a concrete deck (Fig. 2.40).

It can be noticed that the specimens with an axial force in the upright of 25 and 50 kN exhibited a similar initial stiffness, as shown in Figs. 2.39 and 2.40. The ductility of the connection decreases when the axial force is increased. Nevertheless, those specimens, like SBCB-1 and ASBCBF25-1 or CBCBF25-1, that suffered a premature collapse due to weld fracture, showed a lower ductility than the specimens with an axial force of 50 kN.

The increase of the axial force in the upright resulted in a decrease of resistance of the specimens.

Specimen ASBCBF25-1, bolted-and-welded to a steel frame, had a higher initial stiffness and resistance. This was due to the lack of bending in the base of the column.

The collapse modes in the cross-aisle resulted mostly of the weld failure, base bending and distortion buckling of the upright cross section. In Table 2.12 it can be observed that, for the specimens without axial force or with an axial force of 25 kN, the collapse modes were weld failure and base bending. Rotation capacity of those specimens suffering weld failure is heavily reduced.

In no one of the specimens with an axial force of 50 and 75 kN failure due to weld failure or base bending could be observed. The typical collapse mode was distortion buckling of the upright cross section. Figure 2.41 shows each collapse mode mentioned in Table 2.12.

2.3.1.1.2 Bolts in the Compression Zone

Table 2.13 summarizes the results of monotonic tests carried out in cross-aisle direction on column-base connections, with anchor bolts in the compression zone. Also in this case different values of the axial load were considered (0, 25, 50 and 75 kN) as well as different types of connection of the upright steel base to the floor: bolted to a steel or to a concrete floor, as well as bolted-and-welded to a steel deck (as in the Athens dynamic shaking table tests).

Table 2.12 Monotonic tests on column-bases bent in cross-aisle direction with bolts in tension: (a) bolted to a steel surface, (b) bolted to a concrete surface (c) bolted-and-welded to a steel surface

	Axial load [kN]	M_y [kNm]	ϕ_y [mrad]	$S_{j,ini}$ [kNm/rad]	M_{max} [kNm]	ϕ_{max} [mrad]	E_{max} [kNm*mrad]	Failure mode
(a) Steel base								
sbcb-1	0	1.73	24.5	70.4	1.83	41.7	50.5	Weld failure
sbcb-2	0	2.15	41.4	51.9	2.59	178.0	344.4	Base bending
sbcb-3	0	2.34	27.0	86.6	2.44	46.7	59.8	Weld failure
sbcb-4	0	2.25	36.9	60.9	2.86	175.2	388.5	Base bending
sbcb-5	0	2.55	44.1	57.9	3.24	179.6	446.8	Base bending
Average	**0**	**2.20**	**34.8**	**65.5**	**2.59**	**124.2**		**All**
Average	**0**	**2.04**	**25.8**	**78.5**	**2.14**	**44.2**	**55.2**	**Weld failure**
Average	**0**	**2.32**	**40.8**	**56.9**	**2.89**	**177.6**	**393.2**	**Base bending**
sbcbf25-1	25	1.90	21.6	87.9	2.03	37.3	51.7	Weld failure + Base bending
sbcbf25-2	25	2.06	26.4	77.9	2.26	62.5	89.3	Weld failure + Base bending
Average	**25**	**1.98**	**24.0**	**82.9**	**2.14**	**49.9**	**70.5**	**Weld failure + Base bending**
sbcbf50-1	50	1.98	22.9	86.4	2.09	42.0	58.0	Distorsional buckling
sbcbf50-2	50	1.52	14.4	106	1.69	34.6	40.8	Distorsional buckling
Average	**50**	**1.75**	**18.7**	**96.2**	**1.89**	**38.3**	**49.4**	**Distorsional buckling**
(b) Concrete base								
cbcbf25-1	25	1.74	24.9	70.1	1.87	42.6	54.0	Weld failure
cbcbf25-2	25	1.55	22.5	69.0	1.75	56.8	70.8	Weld failure + Base bending
Average	**25**	**1.65**	**23.7**	**69.6**	**1.81**	**49.7**	**62.4**	**All**

(continued)

Table 2.12 (continued)

	Axial load [kN]	M_y [kNm]	ϕ_y [mrad]	$S_{j,ini}$ [kNm/rad]	M_{max} [kNm]	ϕ_{max} [mrad]	E_{max} [kNm*mrad]	Failure mode
cbcbf50-1	50	1.42	17.2	82.6	1.55	36.4	39.0	Distorsional buckling
cbcbf50-2	50	1.89	32.7	57.8	1.96	45.8	54.4	Distorsional buckling
Average	**50**	**1.66**	**25.0**	**70.2**	**1.76**	**41.1**	**46.7**	**Distorsional buckling**
cbcbf75-1	75	0.54	12.4	43.6	0.58	21.4	8.3	Distorsional buckling
	75	**0.54**	**12.4**	**43.6**	**0.58**	**21.4**	**8.3**	
(c) Athen base (bolted + welded)								
asbcbf25-1	25	2.37	29.0	81.8	2.46	46.5	64.2	Weld failure
	25	**2.37**	**29.0**	**81.8**	**2.46**	**46.5**	**64.2**	

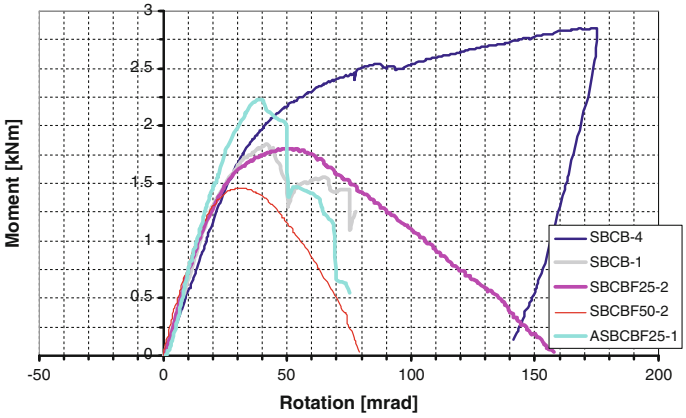

Fig. 2.39 Comparison of the moment-rotation curves for column-base connections bent in cross-aisle direction, with anchor bolts in tension, connected to a steel deck, under different values of the axial load

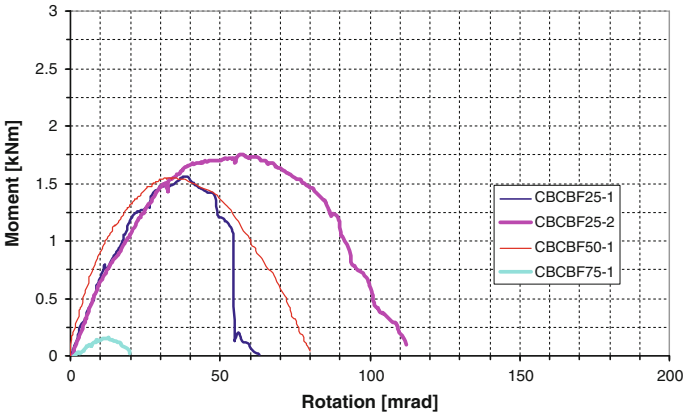

Fig. 2.40 Comparison of the moment-rotation curves for column-base connections bent in cross-aisle direction, with anchor bolts in tension, connected to a concrete deck, under different values of the axial load

Table 2.13 summarizes, for the different types of connections, and for each test, the yield bending moment M_y and rotation ϕ_y, the initial elastic stiffness $S_{j,ini}$, the maximum bending moment M_{max} and associated rotation ϕ_{max}, the energy absorbed up to the attainment of the maximum rotation ϕ_{max}, as well as the failure mode exhibited by the specimen.

Figures 2.42 and 2.43 show a comparison of the moment-rotation curves for column-base connections, with anchor bolts in tension, under different values of the

Fig. 2.41 Collapse modes for specimens bent in cross-aisle direction with bolts in tension

axial load, connected respectively to a steel deck (Fig. 2.42) and to a concrete deck (Fig. 2.43).

In the tests in cross-aisle with bolts in the compression zone, increasing the axial force resulted in an increase of the initial stiffness $S_{j,ini}$, and resistance of the connection, but in a reduction of its ductility.

In the specimen bolted-and-welded to a steel plate (ASBCTF25-1) an increase in the resistance and rotation capacity of the connection was observed, as expected.

Distortional buckling of the upright cross section was not exhibited by any test. The collapse mode for all specimens, except for the ones with bolted-and-welded base, was bending of the base plate, as shown in Fig. 2.44. The magnitude of the uplift of the edges of the base plate, under different values of the axial force is shown in Fig. 2.45. It is possible to observe that higher axial forces correspond to lower base bending.

Table 2.13 Monotonic tests on column-bases bent in cross-aisle direction with bolts in compression zone: (a) bolted to a steel surface, (b) bolted to a concrete surface (c) bolted-and-welded to a steel surface

	Axial load [kN]	M_y [kNm]	ϕ_y [mrad]	$S_{j,ini}$ [kNm/rad]	M_{max} [kNm]	ϕ_{max} [mrad]	E_{max} [kNm mrad]	Failure mode
(a) Steel base								
sbct-1	0	−0.74	−44.7	16.6	−0.91	−199.6	145.8	Base bending
sbct-2	0	−0.62	−68.4	9.1	−0.74	−191.9	104.9	Base bending
sbct-3	0	−0.67	16.2	41.4	−1.03	−199.2	173.9	Base bending
sbct-4	0	−0.65	−25.4	25.6	−0.92	−184.9	138.1	Base bending
sbct-5	0	−0.64	−31.5	20.3	−0.85	183.7	126.2	Base bending
Average	**0**	**−0.66**	**−30.8**	**22.6**	**−0.89**	**−118.4**	**137.8**	**Base bending**
sbctf25-1	25	−0.72	−21.1	34	−0.75	−32.7	16.4	Base bending
sbctf25-2	25	−0.91	−20.6	44	−0.97	−37.8	25.4	Base bending
Average	**25**	**−0.82**	**−20.9**	**39**	**−0.86**	**−35.2**	**20.9**	**Base bending**
sbctf50-1	50	−1.07	−17.7	60.7	−1.13	−27.3	21.4	Base bending
sbctf50-2	50	−1.07	−29.5	36.1	−1.09	−37.5	24.2	Base bending
Average	50	−1.07	−23.6	48.4	−1.11	−32.4	22.8	Base bending
(b) Concrete base								
cbctf25-1	25	−0.80	−10.1	79.0	−0.90	−29.1	20.3	Base bending
	25	**−0.80**	**−10.1**	**79.0**	**−0.90**	**−29.1**	**20.3**	
cbctf50-1	50	−0.95	−12.4	77.0	−1.08	−32.0	24.6	Base bending + Local buckling
	50	**−0.95**	**−12.4**	**77.0**	**−1.08**	**−32.0**	**24.6**	
cbctf75-1	75	−1.04	−9.9	105.2	−1.23	−29.8	26.1	Base bending + Local buckling

(continued)

Table 2.13 (continued)

	Axial load [kN]	M_y [kNm]	ϕ_y [mrad]	$S_{j,ini}$ [kNm/rad]	M_{max} [kNm]	ϕ_{max} [mrad]	E_{max} [kNm mrad]	Failure mode
	75	**−1.04**	**−9.9**	**105.2**	**−1.23**	**−29.8**	**26.1**	
(c) Athen base (bolted + welded)								
asbctf25-1	25	−0.96	−26.8	35.9	−1.14	−76.1	60.0	Weld failure + Local buckling
	25	**−0.96**	**−26.8**	**35.9**	**−1.14**	**−76.1**	**60.0**	

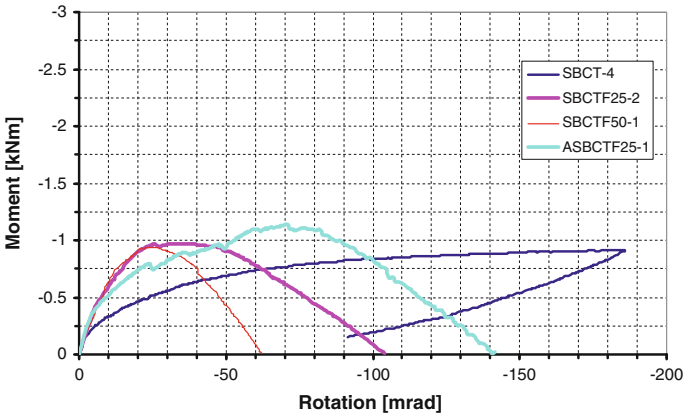

Fig. 2.42 Comparison of the moment-rotation curves for column-base connections bent in cross-aisle direction, with anchor bolts in compression zone, connected to a steel deck, under different values of the axial load

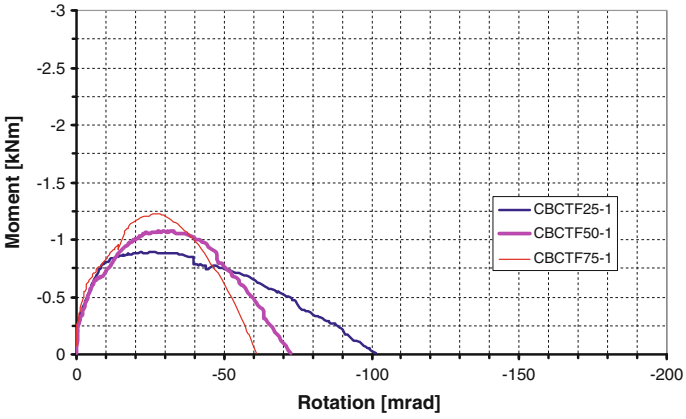

Fig. 2.43 Comparison of the moment-rotation curves for column-base connections bent in cross-aisle direction, with anchor bolts in compression zone, connected to a concrete deck, under different values of the axial load

No base plate bending was observed in the case of bolted-and-welded connections.

2.3.1.2 Down-Aisle

Table 2.14 summarizes the results of monotonic tests carried out on column-base connections in down-aisle direction.

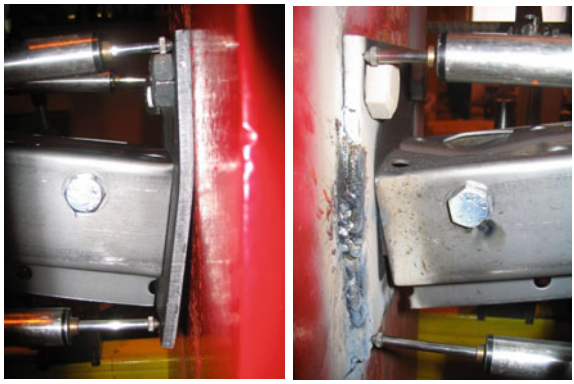

Fig. 2.44 Typical collapse modes for specimens bent in cross-aisle direction with bolts in the compression zone

Also in this case different values of the axial load were considered (0, 25, 50 and 75 kN) as well as different types of connection of the upright steel base to the floor: bolted to a steel or to a concrete floor, as well as bolted-and-welded to a steel deck (as in the Athens dynamic shaking table tests).

Table 2.14 summarizes, for the different types of connections, and for each test, the yield bending moment M_y and rotation ϕ_y, the initial elastic stiffness $S_{j,ini}$, the maximum bending moment M_{max} and associated rotation ϕ_{max}, the energy absorbed up to the attainment of the maximum rotation ϕ_{max}, as well as the failure mode exhibited by the specimen.

Figures 2.46 and 2.47 show a comparison of the moment-rotation curves for column-base connections in down-aisle bending, under different values of the axial

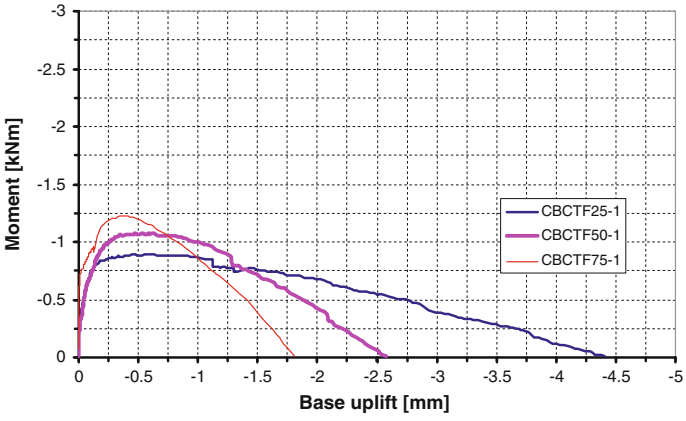

Fig. 2.45 Comparison of the moment-uplift curves for column-base connections bent in cross-aisle direction, with anchor bolts in compression zone, connected to a concrete deck, under different values of the axial load

Table 2.14 Monotonic tests on column-bases bent in down-aisle direction: (a) bolted to a steel surface, (b) bolted to a concrete surface (c) bolted-and-welded to a steel surface

	Axial load [kN]	M_y [kNm]	ϕ_y [mrad]	$S_{j,ini}$ [kNm/rad]	M_{max} [kNm]	ϕ_{max} [mrad]	E_{max} [kNm mrad]	Failure mode
(a) Steel base								
sbdb-1	0	1.66	28.3	58.7	1.70	30.2	31.9	Weld failure
sbdb-2	0	1.46	17.8	81.8	2.04	79.1	118.7	Weld failure
sbdb-3	0	1.95	40.2	48.5	2.36	140.9	254.7	Base bending
sbdb-4	0	1.06	19.3	55.0	1.16	46.1	41.0	Weld failure
sbdb-5	0	1.90	42.1	45.2	2.44	167.4	294.6	Base bending
Average	**0**	**1.61**	**29.5**	**57.8**	**1.94**	**92.7**	**148.2**	**All**
Average	**0**	**1.39**	**21.8**	**65.2**	**1.63**	**51.8**	**63.9**	**Weld failure**
Average	**0**	**1.93**	**41.2**	**46.9**	**2.40**	**154.2**	**274.7**	**Base bending**
sbdbf25-1	25	1.76	13.0	135.7	1.83	25.1	34.7	Base bending
sbdbf25-2	25	1.82	18.4	98.7	2.00	37.3	52.4	Base bending
sbdbf25-3	25	1.30	13.0	99.8	1.42	25.2	23.3	Weld failure
Average	**25**	**1.63**	**14.8**	**111.4**	**1.75**	**29.2**	**36.8**	**All**
Average	**25**	**1.30**	**13.0**	**99.8**	**1.42**	**25.2**	**23.3**	**Weld failure**
Average	**25**	**1.79**	**15.7**	**117.2**	**1.92**	**31.2**	**43.5**	**Base bending**
sbdbf50-1	50	1.65	14.4	114.4	1.82	31.5	40.8	
sbdbf50-2	50	2.49	14.5	172.0	2.61	26.7	51.8	Distorsional buckling + base bending
Average	**50**	**2.07**	**14.5**	**143.2**	**2.21**	**29.1**	**46.3**	
(b) Concrete base								
cbdb-1	0	1.57	27.7	56.6	2.37	173.9	305.1	Base bending
	0	**1.57**	**27.7**	**56.6**	**2.37**	**173.9**	**305.1**	

(continued)

Table 2.14 (continued)

	Axial load [kN]	M_y [kNm]	ϕ_y [mrad]	$S_{j,ini}$ [kNm/rad]	M_{max} [kNm]	ϕ_{max} [mrad]	E_{max} [kNm mrad]	Failure mode
cbdbf25-1	25	1.50	12.9	116.2	1.69	31.5	38.1	Base bending
cbdbf25-2	25	1.47	17.9	81.9	1.58	43.7	49.6	Base bending
Average	**25**	**1.49**	**15.4**	**99.1**	**1.63**	**37.6**	**43.8**	**Base bending**
cbdbf50-1	50	2.09	11.5	181.7	2.26	25.1	41.7	Distorsional buckling + base bending
cbdbf50-2	50	1.94	11.2	173.6	2.15	23.6	37.5	Distorsional buckling + base bending
cbdbf50-3		1.87	11.2	167.3	2.04	25.5	39.5	Distorsional buckling + base bending
Average	**50**	**1.97**	**11.3**	**174.2**	**2.15**	**24.7**	**39.5**	**Distorsional buckling + base bending**
cbdbf75-1	75	1.62	8.4	191.9	1.76	16.5	19.6	Distorsional buckling
	75	**1.62**	**8.4**	**191.9**	**1.76**	**16.5**	**19.6**	
(c) Athen base (bolted + welded)								
asbdbf25-1	25	2.43	21.0	115.6	2.37	60.8	117.0	Bolt slip
	25	**2.43**	**21.0**	**115.6**	**2.37**	**60.8**	**117.0**	

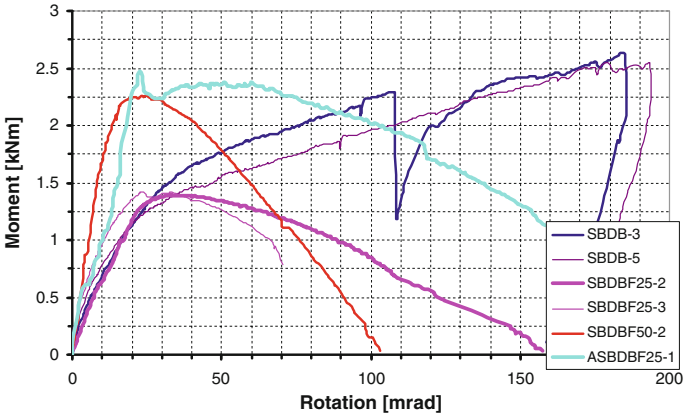

Fig. 2.46 Comparison of the moment-rotation curves for column-base connections bent in down-aisle direction, connected to a steel deck, under different values of the axial load

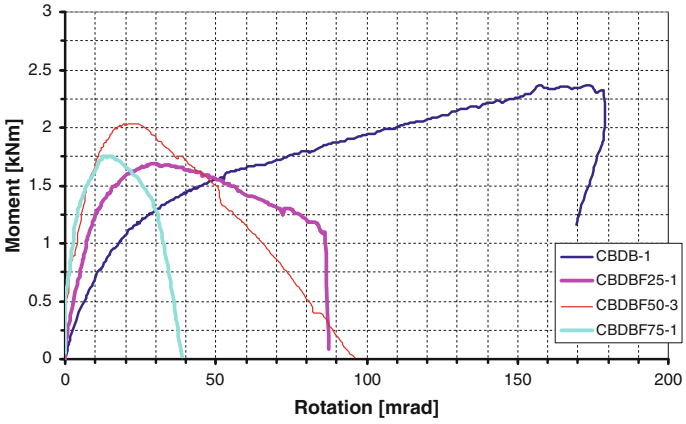

Fig. 2.47 Comparison of the moment-rotation curves for column-base connections bent in down-aisle direction, connected to a concrete deck, under different values of the axial load

load, connected respectively to a steel deck (Fig. 2.46) and to a concrete deck (Fig. 2.47).

The tests performed on column-base connections bent in down-aisle show that the application of an axial force of 25 and 50 kN increases the initial stiffness and resistance, but decreases the rotation capacity of the connection. With an axial force of 75 kN the connection does not exhibit great difference in terms of initial stiffness when compared to the specimen under 50 kN, but both resistance and ductility are lower.

The bolted-and-welded base didn't develop base bending allowing an increase of resistance and rotation capacity of the connection. Figures 2.46 and 2.47 show respectively the moment—rotation curves of the bases connected to the metallic member and to the concrete deck.

The collapse modes exhibited by the specimens under monotonic bending in down-aisle direction were weld failure, base bending and distortion buckling in the cross section of the upright.

The typical collapse mode of the specimens without axial force and with an axial force of 25 kN was base bending. Nevertheless, the specimen SBDBF25-3 exhibited a premature collapse due to weld fracture.

The specimen bolted-and-welded to the steel deck (ASBDBF25-1) evidenced sliding of the bolts connecting the base to the upright, as a consequence of the restraint imposed by the weld to the bending of the base plate.

Specimens with an axial force of 50 kN exhibited distortion buckling of the cross section of the upright associated to base bending. On the other hand, in the tests with an axial force of 75 kN, there was only distortion buckling of the cross section. The typical failure modes of the specimens tested under monotonic bending in down-aisle direction are shown in Fig. 2.48.

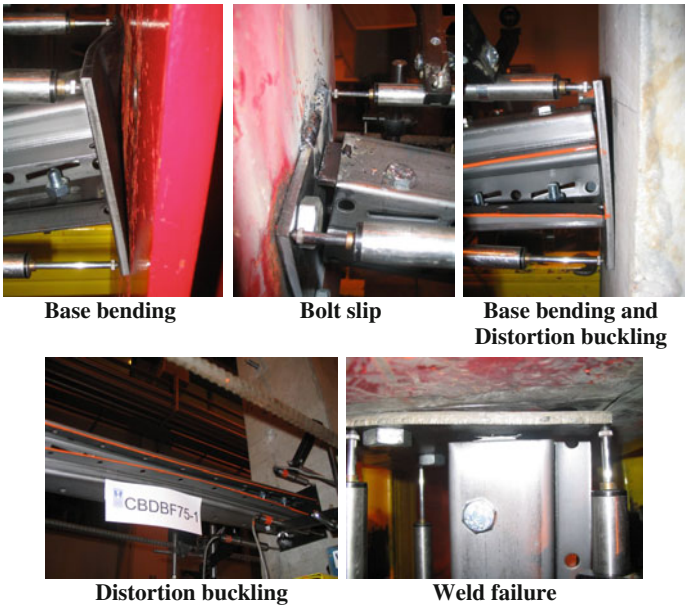

Fig. 2.48 Collapse modes for specimens under monotonic bending in down-aisle direction

2.3.2 Cyclic Tests

2.3.2.1 Cross-Aisle

The cyclic tests on column-base connections under bending in cross-aisle direction were performed considering, as in the monotonic tests, the base plates connected either to the concrete block or to the metallic member (in this case either bolted or bolted-and-welded).

The adopted testing procedure is the one recommended by ECCS (1986).

The tests on the column-base specimens connected to the concrete block (this being the most frequent application in real practice) were performed considering three different values of the compressive axial force, namely 25, 50 and 75 kN (corresponding respectively to 17, 34 and 52 % of the yield strength of the net section of the upright) as shown in Fig. 2.49. The column-base specimens connected to the steel deck were tested considering only a single axial force value of 25 kN, in order to simulate the testing conditions of the dynamic tests carried out on the shaking table at NTUA.

Figures 2.50 and 2.51 show the hysteresis loops in terms of moment and rotation respectively for the specimen simply bolted (Fig. 2.50) and bolted-and-welded (Fig. 2.51) to the steel surface, considering an axial force of 25 kN.

The hysteresis loops related to specimens under cyclic cross-aisle bending presented hereafter are plotted in such a way that positive bending moments and rotation correspond to tensile forces in the bolts, while negative bending moments and rotations correspond to situations in which bolts are in the compression zone.

The test results are summarized in Table 2.15, where in addition to the elastic parameters (yield moment M_y, yield rotation ϕ_y and initial stiffness $S_{j,ini}$) the number of plastic cycles to failure N_u and the total absorbed energy E_{tot} are also

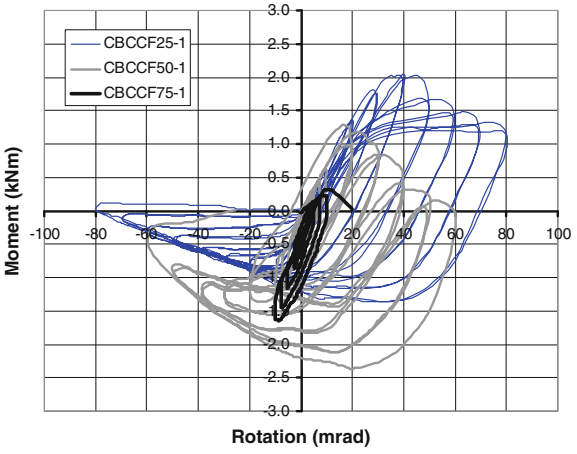

Fig. 2.49 Hysteresis loops for specimen connected to a concrete deck, under cyclic bending in cross-aisle direction and different values of the axial load

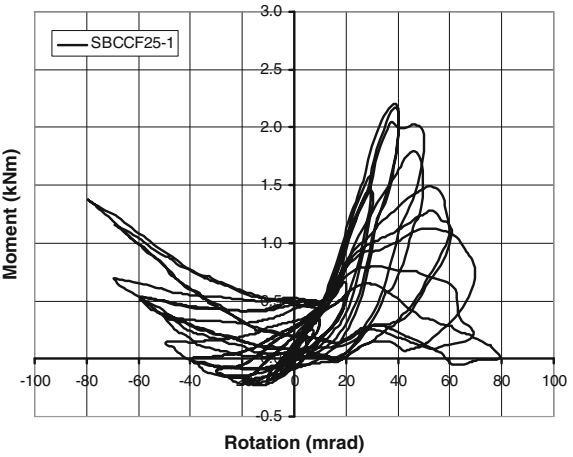

Fig. 2.50 Hysteresis loops for the specimen connected to a steel deck, under cyclic bending in cross-aisle direction

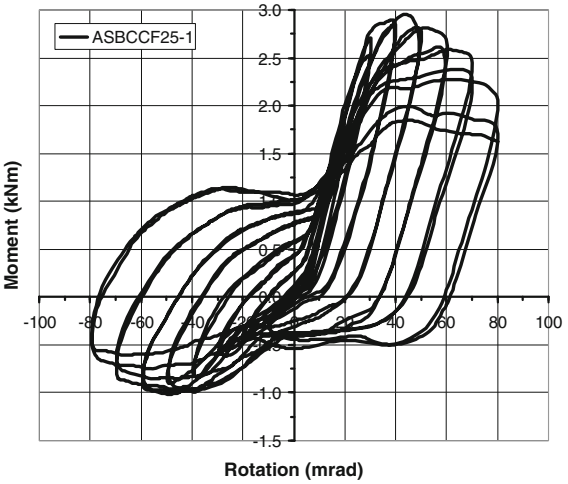

Fig. 2.51 Hysteresis loops for the specimen bolted-and-welded to a steel deck, under cyclic bending in cross-aisle direction

Table 2.15 Cyclic tests on column-bases bent in cross-aisle direction

	Base	Axial load [kN]	M_y [kNm]	ϕ_y [mrad]	$S_{j,ini}$ [kNm/rad]	N_u	E_{tot} [kNm mrad]
asbccf25-1	Athens	25	2.83	33.0	85.9	10	1756
sbccf25-1	Steel	25	1.45	20.0	72.4	8	496
cbccf25-1	Concrete	25	2.00	26.3	75.8	12	1305
cbccf50-1	Concrete	50	0.92	10.3	89.7	9	634
cbccf75-1	Concrete	75	0.31	3.5	89.2	1	27.8

presented. Assessment of the number of cycles to failure was performed according to (Bernuzzi et al. 1997a, 2000).

Collapse of specimens with axial force of 25 kN was due to base bending under negative bending moments (when bolts are in the compression zone).

For specimens with an axial force of 50 and 75 kN (Fig. 2.49), collapse occurred as a consequence of distortion buckling of the cross section of the upright. As in the monotonic tests, the higher the axial force, the lower the strength of the specimen under positive bending moments (bolts in tension). On the other hand, presence of the axial force is beneficial to the resistance of the specimens, reducing the base bending deformation that develops when the base is under negative bending moments, with bolts in the compression zone.

Specimen CBCCF75-1 exhibited a very low load carrying capacity when the base was under negative bending with bolts in the compression zone, due to evident distortion buckling. Consequently, the test was stopped at the first plastic cycle.

Welding between the base and the steel deck increased the resistance of specimen ASBCCF25-1 (Fig. 2.51). The shape of the half cycle with negative bending moment is different when compared to those of specimens CBCCF25-1 (Fig. 2.49) and SBCCF25-1 (Fig. 2.50). This difference is due to the lack of bending deformation of the base plate, that is restrained by the fillet welds, and allows an increase of dissipated energy.

2.3.2.2 Down-Aisle

As in the case of cross-aisle testing, also the cyclic tests on column-base connections under bending in down-aisle direction were performed considering the base connected either to a concrete block or to a metallic member (in this case either bolted or bolted-and-welded).

The adopted testing procedure is the one recommended by ECCS (1986).

The tests on the column-base specimens connected to the concrete block (being the most frequent application in real practice) were performed considering three values of the compressive axial force: 25, 50 and 75 kN, as shown in Fig. 2.53. The column-base specimens connected to the steel deck were tested considering only an axial force of 25 kN, in order to simulate the testing conditions of the dynamic tests carried out on the shaking table at NTUA.

Figures 2.52 and 2.54 show the hysteresis loops in terms of moment and rotation respectively for the specimen simply bolted (Fig. 2.52) and bolted-and-welded (Fig. 2.54) to the steel surface, considering an axial force of 25 kN.

The test results are summarized in Table 2.16, where in addition to the elastic parameters (yield moment M_y, yield rotation ϕ_y and initial stiffness $S_{j,ini}$) the number of plastic cycles to failure N_u and the total absorbed energy E_{tot} are also presented.

Despite of the geometrical symmetry of the column base in this loading configuration, the load carrying capacity of the specimens under negative bending moment is slightly higher than that exhibited under positive bending.

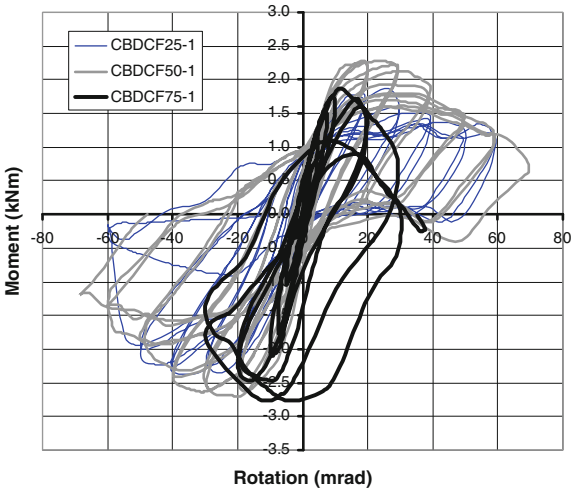

Fig. 2.52 Hysteresis loops for specimens connected to a concrete deck, under cyclic bending in down-aisle direction and different values of the axial load

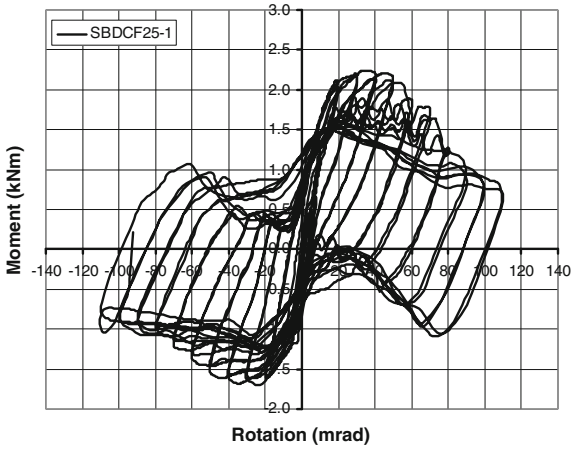

Fig. 2.53 Hysteresis loops for the specimen connected to a steel deck, under cyclic bending in down-aisle direction

This is probably due to the combined effect of the axial load superimposed to an initial out-of-straightness of the specimens, caused by the gravity load of the test apparatus (approximately estimated in 0.3 kN), that resulted in second order effects, leading to an un-symmetric response of the specimens, that enhanced when increasing the axial force.

In any case, the axial load improved the load carrying capacity of the column base under both positive and negative bending. This was true for all specimens, with the exception of CBDCF75-1 (Fig. 2.53) due to the premature distortional buckling of the upright cross section.

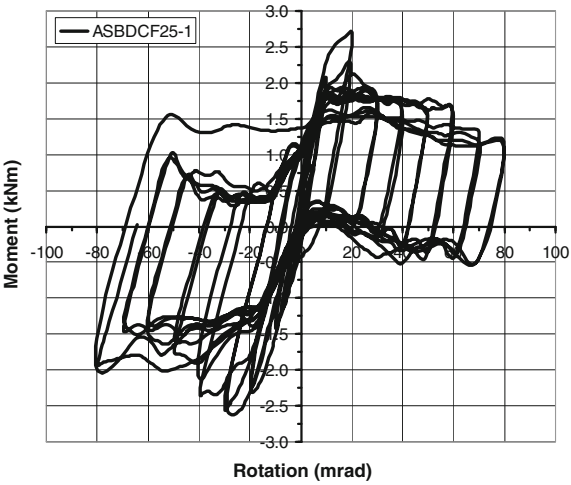

Fig. 2.54 Hysteresis loops for the specimen bolted-and-welded to a steel deck, under cyclic bending in down-aisle direction

Table 2.16 Cyclic tests on column-bases bent in down-aisle direction

	Base	Axial load [kN]	M_y [kNm]	ϕ_y [mrad]	$S_{j,ini}$ [kNm/rad]	N_u	E_{tot} [kNm mrad]
asbdcf25-1	Athens	25	2.57	15.4	167.4	14	2123
sbdcf25-1	Steel	25	1.94	15.0	129.7	20	3460
cbdcf25-1	Concrete	25	1.75	20.7	84.8	8	806
cbdcf50-1	Concrete	50	2.17	12.8	169.4	11	1196
cbdcf75-1	Concrete	75	1.80	9.5	190.7	6	389

The base plate welded and bolted to the metallic deck (specimen ASBDCF25-1, Fig. 2.54) improved the resistance, stiffness and energy dissipation capacity of the connection, when compared to the specimen simply bolted to the steel deck (specimen SBDCF25-1, Fig. 2.52). Weld failure, however occurred in specimen ASBDCF25-1 after 14 plastic cycles, under a maximum rotation of 80 mrad, while specimen SBDCF25-1, simply bolted to the steel deck, sustained 20 cycles in the plastic range, with a maximum rotation capacity of approximately 110 mrad, and consequently a larger total absorbed energy E_{tot}.

Specimen CBDCF25-1 collapsed due to weld failure, while specimen CBDCF50-1 collapsed due to plate bending and onset of distortional buckling in the upright cross section.

2.3.3 Comparison and Analysis of Test Results

2.3.3.1 Monotonic Tests

Figures 2.55, 2.56, 2.57, 2.58 and 2.59 show a comparison of the response, in terms of moment-rotation curves, of column-base connections for different directions of bending, under similar conditions of applied axial load and "deck connection".

Figure 2.55 refers to specimens without axial load and connected to a steel deck. Figures 2.56, 2.57 and 2.58 present the results for specimens connected to a concrete deck, respectively with 25, 50 and 75 kN axial load, while Fig. 2.59 refers to specimens with 25 kN axial load bolted-and-welded to a steel deck.

Tables 2.17 and 2.18 show a comparison of the mean values of the results of monotonic tests on column-base connections bent in cross-aisle direction, respectively with bolts in tension (Table 2.17) and in compression (Tables 2.18), while Table 2.19 refers to the case of down-aisle bending. Each table shows the comparison of the results obtained for different types of deck connection (namely bolted to a concrete deck (b) and either bolted (a) or bolted-and-welded (c) to a steel deck).

Table 2.20 shows a comparison of the mean values of the results obtained in monotonic tests on column-bases bent in cross-aisle direction with bolts in tension versus bolts in compression zone. Similarly, Table 2.21 compares the results of cross-aisle bending with bolts in tension with those of down-aisle bending, while Table 2.22 compares the results of down-aisle bending with those of cross-aisle bending with bolts in compression.

Examining Table 2.17 it can be noticed that in monotonic bending tests with bolts in tension, increasing the axial load in the column always results in an increment of stiffness but in a reduction of strength, ductility and energy absorption capacity of the specimens bolted either to a steel or a concrete deck. Bolting and welding the specimens to a steel surface is always beneficial with respect to simply bolting to either a concrete or a steel deck, under the same axial load.

In monotonic bending tests with bolts in the compression zone (Table 2.18), increasing the axial load in the column results in an increment of stiffness, strength,

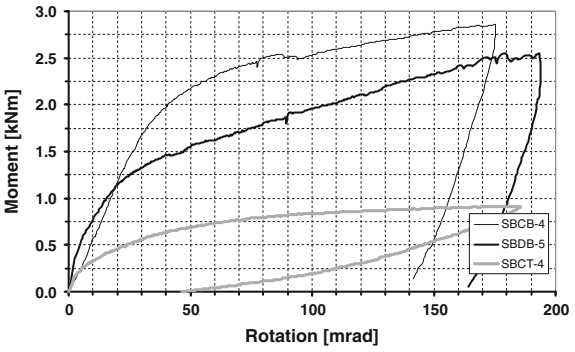

Fig. 2.55 Comparison of the moment-rotation curves for column-base connections, without axial load and connected to a steel deck, for different directions of bending

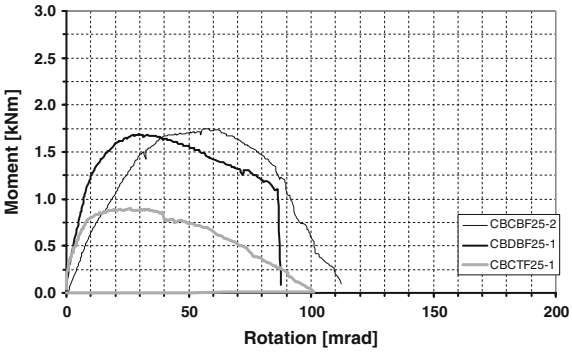

Fig. 2.56 Comparison of the moment-rotation curves for column-base connections, with 25 kN axial load and connected to a concrete deck, for different directions of bending

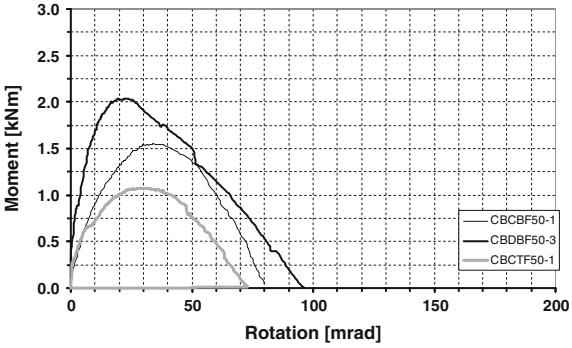

Fig. 2.57 Comparison of the moment-rotation curves for column-base connections, with 50 kN axial load and connected to a concrete deck, for different directions of bending

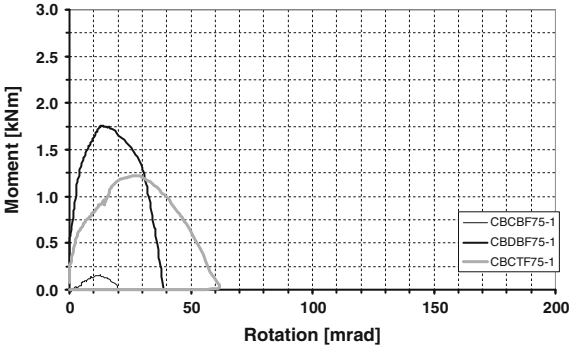

Fig. 2.58 Comparison of the moment-rotation curves for column-base connections, with 75 kN axial load and connected to a concrete deck, for different directions of bending

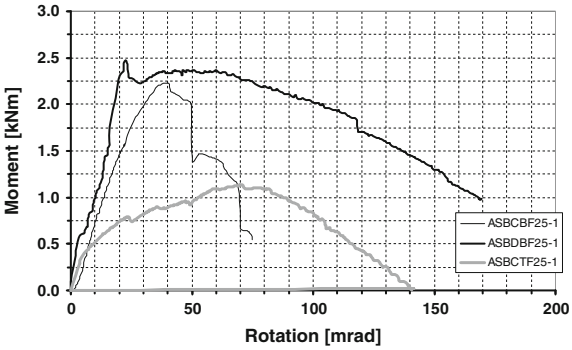

Fig. 2.59 Comparison of the moment-rotation curves for column-base connections, with 25 kN axial load bolted-and-welded to a steel deck, for different directions of bending

Table 2.17 Comparison of the results of monotonic tests on column-bases bent in cross-aisle direction, with bolts in tension

M_y	ϕ_y	$S_{j,ini}$	M_{max}	ϕ_{max}	E_{max}	
(a) Steel base						
1.14	1.58	0.72	1.35	4.02	7.12	sbcb Base bending/weld failure
0.95	0.85	1.15	0.90	0.70	0.66	sbcb All/base bending
1.08	1.35	0.83	1.21	2.81	4.67	sbcb All/weld failure
0.90	0.69	1.27	0.83	0.40	0.27	sbcbf25 /sbcb
0.88	0.78	1.16	0.88	0.77	0.70	sbcbf50 /sbcbf25
0.80	0.54	1.47	0.73	0.31	0.19	sbcbf50 /sbcb
(b) Concrete base						
1.01	1.05	1.01	0.97	0.83	0.75	cbcbf50 /cbcbf25
0.33	0.50	0.62	0.33	0.52	0.18	cbcbf75 /cbcbf50
0.33	0.52	0.63	0.32	0.43	0.13	cbcbf75 /cbcbf25
(c) Athen base (bolted + welded)						
1.20	1.21	0.99	1.15	0.93	0.91	asbcbf25/sbcbf25
1.44	1.22	1.18	1.36	0.94	1.03	asbcbf25/cbcbf25

ductility and energy absorption capacity of the specimens bolted a concrete deck. On the contrary, for specimens bolted to a steel deck, increasing the axial load results in an increment of stiffness and strength, but in a reduction of ductility and energy absorption capacity. Bolting and welding the specimens to a steel surface is always beneficial with respect to strength, ductility and energy absorption capacity with respect to simply bolting either to a concrete or to a steel deck, under the same axial load.

Table 2.18 Comparison of the results of monotonic tests on column-bases bent in cross-aisle direction, with bolts in compression zone

M_y	ϕ_y	$S_{j,ini}$	M_{max}	ϕ_{max}	E_{max}	
(a) Steel base						
1.24	0.68	1.73	0.97	0.30	0.15	sbctf25 /sbct
1.30	1.13	1.24	1.29	0.92	1.09	sbctf50 /sbctf25
1.62	0.77	2.14	1.25	0.27	0.17	sbctf50 /sbct
(b) Concrete base						
1.19	1.23	0.97	1.20	1.10	1.21	cbctf50 /cbctf25
1.09	0.80	1.37	1.14	0.93	1.06	cbctf75 /cbctf50
1.30	0.98	1.33	1.37	1.02	1.29	cbctf75 /cbctf25
(c) Athen base (bolted + welded)						
1.17	1.28	0.92	1.33	2.16	2.87	asbctf25/sbctf25
1.20	2.65	0.45	1.27	2.62	2.96	asbctf25/cbctf25

In the case of monotonic bending in down-aisle direction (Table 2.19) it can be noticed that increasing the axial load results in an increment of strength and stiffness, but in a reduction of ductility and energy absorption capacity for specimens bolted to a steel deck. When specimens are bolted to a concrete surface, increasing the axial load results in an increment of stiffness, a reduction of ductility and energy absorption capacity, while strength increases for low and intermediate values of the applied axial force (up to 50 kN), but reduces for higher values of the axial load (75 kN).

Bolting and welding the specimens to a steel surface is, in this loading direction, always beneficial for stiffness, strength, ductility and energy absorption capacity with respect to simply bolting either to a concrete or to a steel deck, under the same axial load.

When comparing the main response parameters of monotonic tests in cross-aisle bending with bolts in tension with the corresponding parameters related to tests performed with bolts in compression zone (Table 2.20), it can be noticed that the yield and maximum bending moments as well as the maximum absorbed energy of tests performed with bolts in tension are always larger than those of tests performed with bolts in compression zone, when the axial load is less than 75 kN.

The yield and maximum rotation of specimens tested with bolts in tension are always larger than those of tests performed with bolts in compression zone, with the exception of specimens bolted to a steel deck, under a 50 kN axial load (for which is $\phi_{y,CT} > \phi_{y,CB}$) and of those bolted to a concrete surface with an axial load of 75 kN (for which is $\phi_{max,CT} > \phi_{max,CB}$). Stiffness of specimens connected to a steel deck (simply bolted or bolted-and-welded) tested with bolts in tension was always higher than that of specimens tested with bolts in compression zone. The opposite is true for specimens bolted to a concrete deck, for which $S_{j,ini,CT} > S_{j,ini,CB}$. This is probably due to problems in the bond between the anchor bolts and the concrete or eventually to cracking of the concrete under tensile loads.

Table 2.19 Comparison of the results of monotonic tests on column-bases bent in down-aisle direction

M_y	ϕ_y	$S_{j,ini}$	M_{max}	ϕ_{max}	E_{max}	
(a) Steel base						
1.39	1.89	0.72	1.47	2.98	4.30	sbdb Base bending/weld failure
0.83	0.72	1.23	0.81	0.60	0.54	sbdb All/base bending
1.16	1.35	0.89	1.19	1.79	2.32	sbdb All/weld failure
1.38	1.21	1.17	1.35	1.24	1.87	sbdbf25 Base bending/weld failure
0.91	0.94	0.95	0.91	0.94	0.85	sbdbf25 All/base bending
1.25	1.14	1.12	1.23	1.16	1.58	sbdbf25 All/weld failure
1.01	0.50	1.93	0.90	0.31	0.25	sbdbf25/sbdb All
0.94	0.60	1.53	0.87	0.49	0.36	sbdbf25/sbdb Weld failure
0.93	0.38	2.50	0.80	0.20	0.16	sbdbf25/sbdb Base bending
1.27	0.98	1.29	1.26	1.00	1.26	sbdbf50/sbdbf25
1.29	0.49	2.48	1.14	0.31	0.31	sbdbf50/sbdb
(b) Concrete base						
0.95	0.56	1.75	0.69	0.22	0.14	cbdbf25/cbdb
1.32	0.73	1.76	1.32	0.66	0.90	cbdbf50/cbdbf25
1.25	0.41	3.08	0.91	0.14	0.13	cbdbf50/cbdb
0.82	0.74	1.10	0.82	0.67	0.50	cbdbf75/cbdbf50
1.09	0.55	1.94	1.08	0.44	0.45	cbdbf75/cbdbf25
1.03	0.30	3.39	0.74	0.09	0.06	cbdbf75/cbdb
(c) Athens base (bolted + welded)						
1.49	1.42	1.04	1.35	2.08	3.18	asbdbf25/sbdbf25
1.63	1.36	1.17	1.45	1.62	2.67	asbdbf25/cbdbf25

When comparing the main response parameters of monotonic tests in cross-aisle bending with bolts in tension with the corresponding parameters related to tests performed in down-aisle direction, (Table 2.21) the following considerations can be drawn: stiffness $S_{j,ini}$ in down-aisle direction is always higher than in cross-aisle direction, in presence of axial load in the column. Both the yield M_y and maximum M_{max} bending moments in down-aisle are larger than in cross-aisle, for axial load larger than 25 kN. The yield rotation ϕ_y in cross-aisle direction, with bolts in tension is always larger than that in down-aisle direction. The same consideration is

Table 2.20 Comparison of the results of monotonic tests on column-bases bent in cross-aisle direction: bolts in tension versus bolts in compression

M_y	ϕ_y	$S_{j,ini}$	M_{max}	ϕ_{max}	E_{max}	
(a) Steel base						
3.33	1.13	2.90	2.91	1.05	1.87	sbcb/sbct All
3.52	1.32	2.52	3.25	1.50	2.85	sbcb/sbct Base bending
2.41	1.15	2.13	2.49	1.42	3.37	sbcb25/sbct25
1.64	0.79	1.99	1.70	1.18	2.17	sbcb50/sbct50
(b) Concrete base						
2.06	2.35	0.88	2.01	1.71	3.07	cbcb25/cbct25
1.75	2.02	0.91	1.63	1.28	1.90	cbcb50/cbct50
0.52	1.25	0.41	0.47	0.72	0.32	cbcb75/cbct75
(c) Athen base (bolted + welded)						
2.47	1.08	2.28	2.16	0.61	1.07	asbcb25/asbct25

Table 2.21 Comparison of the results of monotonic tests on column-bases in cross-aisle bending with bolts in tension versus down-aisle bending

M_y	ϕ_y	$S_{j,ini}$	M_{max}	ϕ_{max}	E_{max}	
(a) Steel base						
1.37	1.18	1.13	1.34	1.34	1.74	sbcb/sbdb All
1.47	1.18	1.20	1.31	0.85	0.86	sbcb/sbdb Weld failure
1.20	0.99	1.21	1.20	1.15	1.43	sbcb/sbdb Base bending
1.21	1.62	0.74	1.22	1.71	1.92	sbcb25/sbdb25
0.85	1.29	0.67	0.86	1.32	1.07	sbcb50/sbdb50
(b) Concrete base						
1.10	1.54	0.70	1.11	1.32	1.42	cbcb25/cbdb25
0.84	2.21	0.40	0.82	1.66	1.18	cbcb50/cbdb50
0.33	1.48	0.23	0.33	1.30	0.42	cbcb75/cbdb75
(c) Athen base (bolted + welded)						
0.98	1.38	0.71	1.04	0.76	0.55	asbcb25/asbdb25

true also for the maximum rotation ϕ_{max}, with the exception of the case when the base is bolted-and-welded to the steel deck.

When comparing the main response parameters of monotonic tests in cross-aisle bending with bolts in compression zone, with the corresponding parameters related to tests performed in down-aisle direction (Table 2.22), the following considerations can be drawn: stiffness $S_{j,ini}$ as well as both the yield M_y and maximum M_{max}

Table 2.22 Comparison of the results of monotonic tests on column-bases in down-aisle bending versus cross-aisle bending with bolts in compression

M_y	ϕ_y	$S_{j,ini}$	M_{max}	ϕ_{max}	E_{max}	
(a) Steel base						
2.44	0.96	2.56	2.18	0.78	1.08	sbdb/sbct All
2.92	1.34	2.08	2.70	1.30	1.99	sbdb/sbct Base bending
1.99	0.71	2.86	2.03	0.83	1.76	sbdb25/sbct25
1.93	0.61	2.96	1.99	0.90	2.03	sbdb50/sbct50
(b) Concrete base						
1.86	1.52	1.25	1.81	1.29	2.16	cbdb25/cbct25
2.07	0.91	2.26	1.99	0.77	1.61	cdb50/cbct50
1.56	0.85	1.82	1.43	0.55	0.75	cbdb75/cbct75
(c) Athen base (bolted + welded)						
2.53	0.78	3.22	2.08	0.80	1.95	asbdb25/asbct25

bending moments in down-aisle direction are always higher than in cross-aisle direction. The yield rotation ϕ_y as well as the maximum rotation ϕ_{max}, in cross-aisle direction, with bolts in compression zone, are always larger than those in down-aisle direction, in presence of an axial load in the column. The maximum absorbed energy in down-aisle direction is always larger than in cross-aisle direction, for axial loads lower than 75 kN.

Figures 2.60, 2.61, 2.62, 2.63, 2.64 and 2.65 summarize the previous considerations, plotting the trend of the mean value of the main response parameters of all tests, under increasing the axial load in the column.

As a general consideration, examining Figs. 2.60 to 2.65 it is evident that there is a rather good agreement in the trends of tests performed with specimens bolted to a concrete or to a steel deck. Some scatter is evident, in particular in the case of the initial stiffness (Fig. 2.62), although this is to be expected due to the different behaviour of the anchor bolts, when connected to a steel plate or chemically "bonded" into a concrete block.

It can be observed that the yield moment M_y (Fig. 2.60), in the case of tests in cross-aisle direction with bolts in tension (cbcb and sbcb test series) decreases steadily up to an axial load of 50 kN, and drops abruptly for further increments of the axial load. In the case of tests in cross-aisle direction with bolts in the compression zone (cbct and sbct test series) M_y steadily increases with the axial load, which is beneficial in reducing the base-plate bending effect. In the case of tests in cross-aisle direction (cbdb and sbdb test series) M_y attains a maximum value for an axial load of 50 kN.

Both the yield rotation ϕ_y (Fig. 2.61) and the maximum rotation ϕ_{max} (Fig. 2.64) are always heavily reduced by the application of the axial load, although the value of ϕ_{max} doesn't seem to be much influenced by increment of the axial load beyond

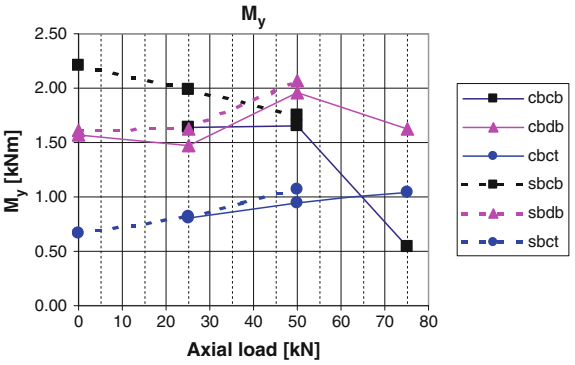

Fig. 2.60 Yield-moment versus axial load for column-base connections

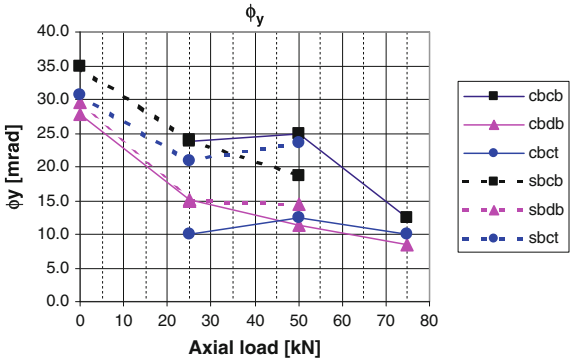

Fig. 2.61 Yield-rotation versus axial load for column-base connections

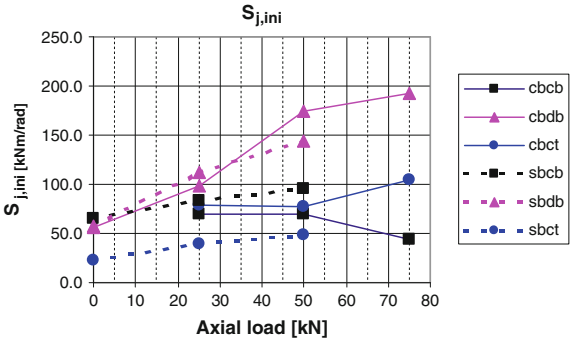

Fig. 2.62 Initial elastic stiffness versus axial load for column-base connections

25 kN. The initial elastic stiffness $S_{j,ini}$ (Fig. 2.62) increases with the axial load in the case of tests in down-aisle bending (cbdb and sbdb test series) and in cross-aisle bending with bolts in the compression zone (cbct and sbct test series). In the case of tests performed in cross-aisle bending with bolts in tension (cbcb and sbcb test series), $S_{j,ini}$ initially moderately increases with the axial load, but diminishes when the applied axial load is increased up to 75 kN.

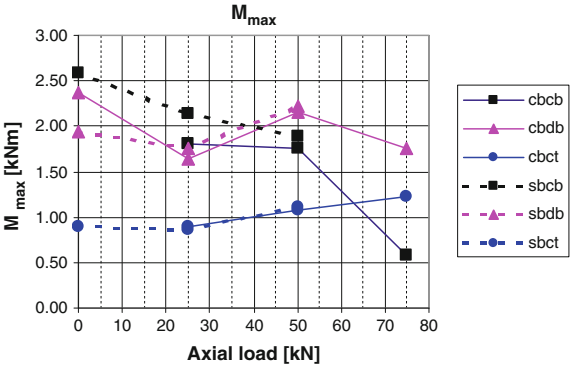

Fig. 2.63 Maximum bending strength versus axial load for column-base connections

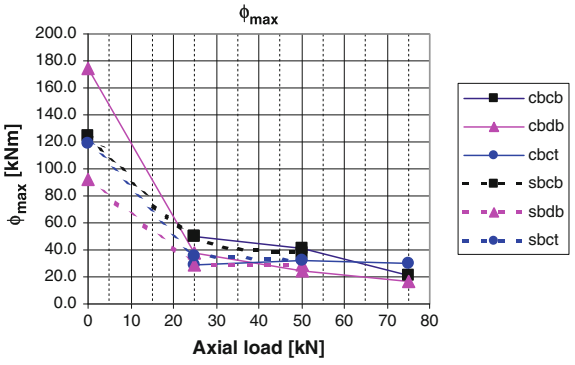

Fig. 2.64 Rotation corresponding to maximum bending strength versus axial load for column-base connections

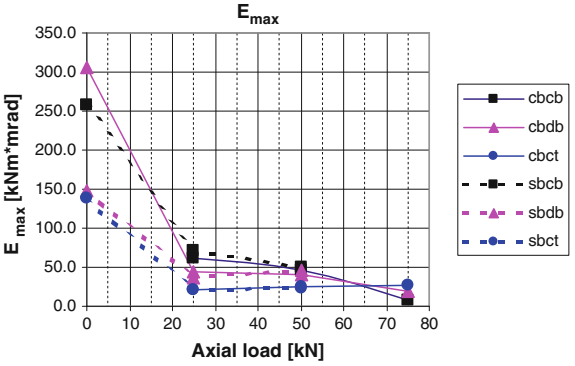

Fig. 2.65 Absorbed energy corresponding to maximum bending strength versus axial load for column-base connections

The maximum bending strength M_{max} (Fig. 2.63), in the case of tests in cross-aisle direction with bolts in tension (cbcb and sbcb test series) decreases steadily up to an axial load of 50 kN, and drops abruptly for further increments of the axial load. This is due to onset of distortion buckling of the cross section of the column. In the case of tests in cross-aisle direction with bolts in compression zone (cbct and sbct test series)

M_{max} steadily increases with the axial load. In the case of tests in cross-aisle direction (cbdb and sbdb test series) M_{max} oscillates around a practically constant value. The same considerations drawn for the maximum rotation ϕ_{max} apply also to the case of the maximum absorbed energy E_{tot} (Fig. 2.65). This parameter is however more sensible to increments of the axial load beyond 50 kN.

2.3.3.2 Cyclic Tests

The following Figs. 2.66, 2.67, 2.68, 2.69, 2.70, 2.71, 2.72, 2.73, 2.74, 2.75 and 2.76 show comparisons of the hysteretic behaviour of the specimens, tested under different loading and/or restraint conditions, in terms of applied bending moment versus rotation.

It should be pointed out that the hysteresis loops related to specimens under cyclic cross-aisle bending presented hereafter are plotted in such a way that positive bending moments and rotation correspond to tensile forces in the bolts, while negative bending moments and rotations correspond to situations in which bolts are in compression zone.

Figures 2.66 to 2.70 present a comparison of the specimens response, under the same axial load, but bent in different directions (namely cross and down-aisle).

Figure 2.66 refers to the specimens simply bolted to the steel deck, with a 25 kN axial load, and shows the poor response in cross-aisle direction of this type of connection, due to the low load carrying capacity when bolts are in the compression zone.

Figures 2.67, 2.68 and 2.69 refer to specimens simply bolted to the concrete deck, respectively with a 25, 50 and 75 kN axial load.

Response in cross-aisle direction of this type of connection, when bolts are in the compression zone, is better than the one evidenced by specimens connected to a

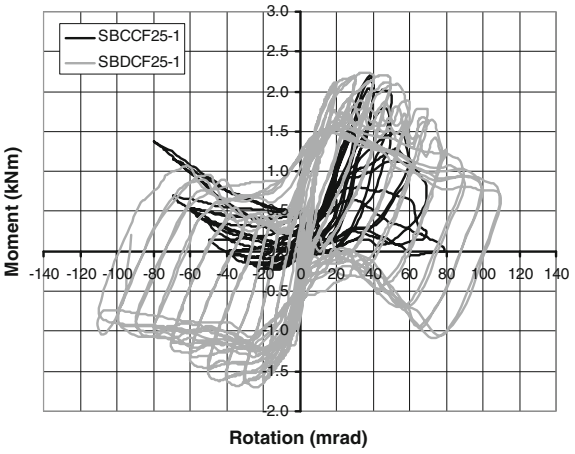

Fig. 2.66 Comparison of the hysteretic behaviour of column-bases connected to a steel deck, with 25 kN axial load, for different bending directions

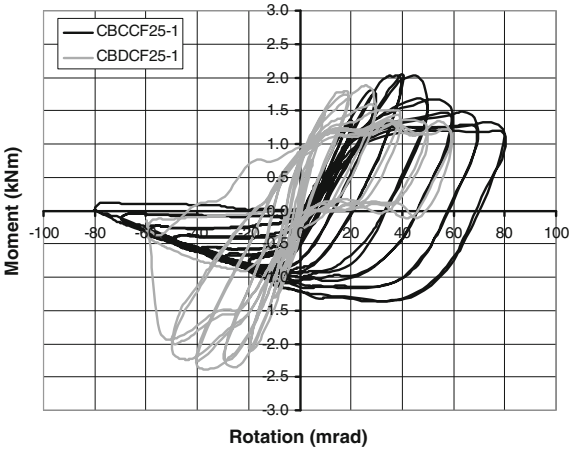

Fig. 2.67 Comparison of the hysteretic behaviour of column-bases connected to a concrete deck, with 25 kN axial load, for different bending directions

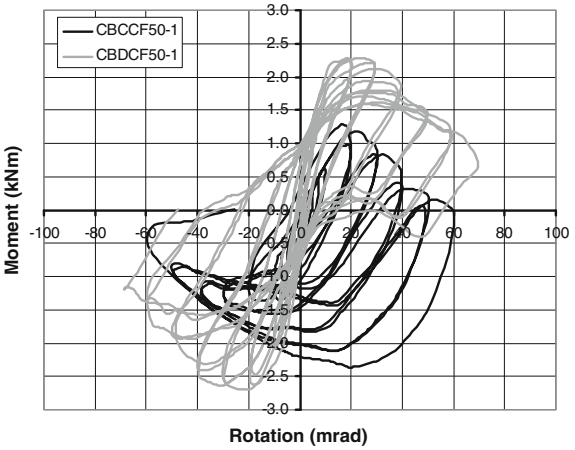

Fig. 2.68 Comparison of the hysteretic behaviour of column-bases connected to a concrete deck, with 50 kN axial load, for different bending directions

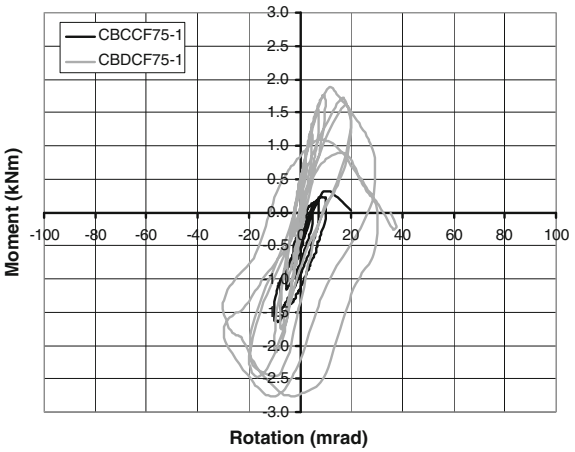

Fig. 2.69 Comparison of the hysteretic behaviour of column-bases connected to a concrete deck, with 75 kN axial load, for different bending directions

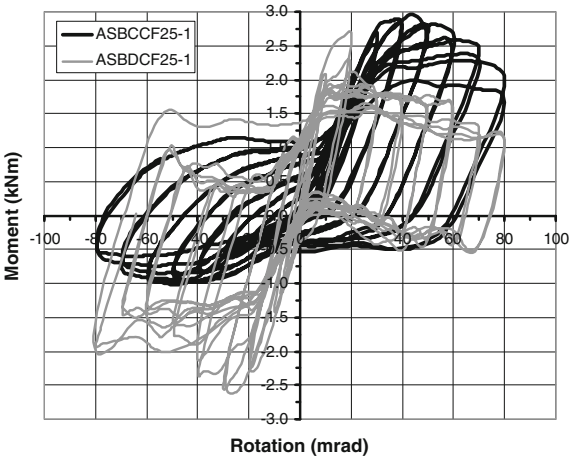

Fig. 2.70 Comparison of the hysteretic behaviour of column-bases bolted-and-welded to a steel deck, with 25 kN axial load, for different bending directions

steel deck, most probably due to the local deformability of the concrete surface, or in any case to the different behaviour at the base-deck interface.

It is also evident that increasing the axial load up to 50 kN is beneficial for the specimen response in down-aisle direction. In cross-aisle direction, increasing the axial load up to 50 kN results in a reduction of rotation capacity. The load carrying capacity is also reduced when bolts are in tension (due to occurrence of buckling at the free edges of the cross section of the column profile which are in compression). On the contrary, the bending strength is improved by increasing the axial load for those conditions in which the bolts are in the compression zone (as, in this case, the axial load reduces the bending deformation of the steel base plate).

Further increasing of the axial load to 75 kN causes a loss of load-carrying as well as rotation capacity of the specimens in both bending directions (as shown in Fig. 2.69).

Figure 2.70 refers to the specimens bolted-and-welded to the steel deck, with a 25 kN axial load, and shows the good response in both cross-aisle and down-aisle direction of this type of connection in terms of both load-carrying and rotation capacity.

Figures 2.71 and 2.72 compare the response of specimens simply bolted and bolted-and-welded to a steel deck, under 25 kN axial load, respectively under bending in cross-aisle and in down-aisle direction. Similarly, Figs. 2.73 and 2.74 compare the response of specimens simply bolted to a concrete floor and bolted-and-welded to a steel deck, under 25 kN axial load, respectively under bending in cross-aisle and in down-aisle direction. The beneficial effect of the bolted-and-welded type of connection is evident, when comparing the behaviour of specimens connected to a steel floor, particularly for cross-aisle bending. When compared to specimens simply bolted to a concrete floor, the response of bolted-and-welded base connections shows a small enhancement of both load-carrying and rotation capacity in down-aisle direction. In cross-aisle direction,

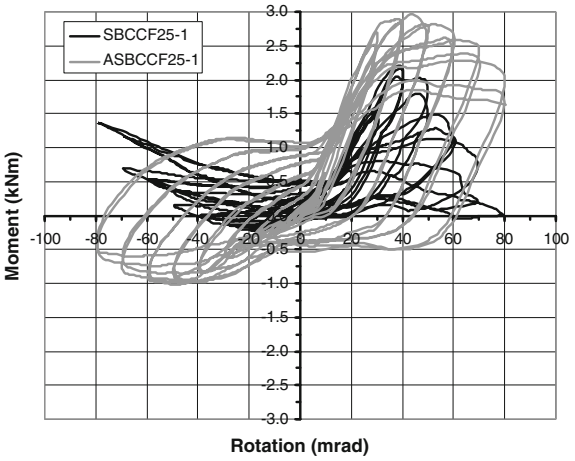

Fig. 2.71 Comparison of the hysteretic behaviour of column-bases, with 25 kN axial load, under cyclic bending in cross-aisle direction, simply bolted and bolted-and-welded to a steel deck

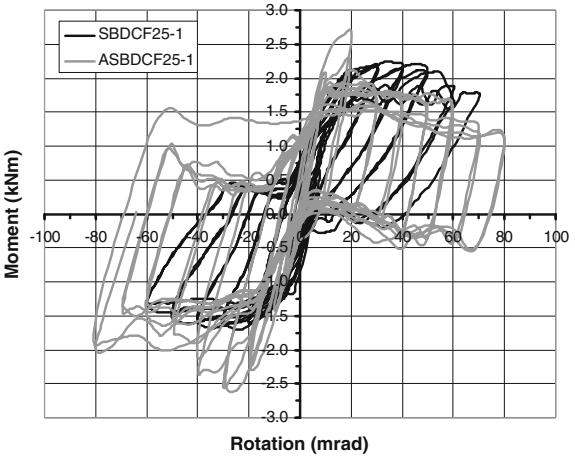

Fig. 2.72 Comparison of the hysteretic behaviour of column-bases, with 25 kN axial load, under cyclic bending in down-aisle direction, simply bolted and bolted-and-welded to a steel deck

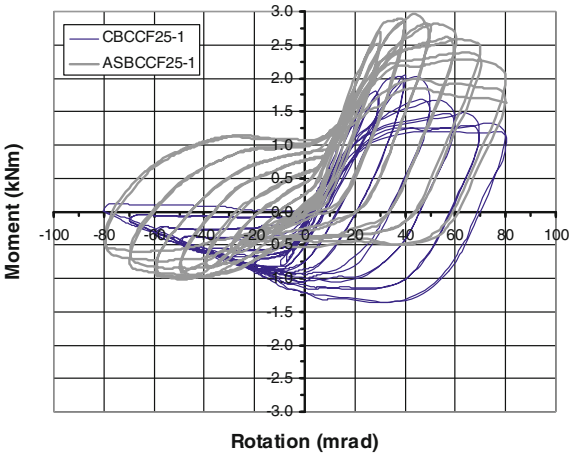

Fig. 2.73 Comparison of the hysteretic behaviour of column-bases, with 25 kN axial load, under cyclic bending in cross-aisle direction, connected to a concrete deck or bolted-and-welded to a steel deck

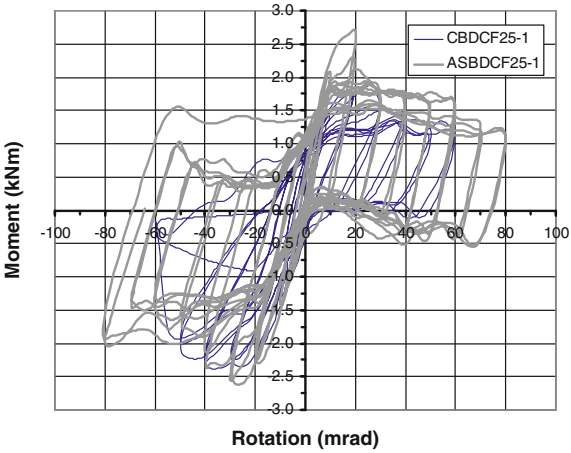

Fig. 2.74 Comparison of the hysteretic behaviour of column-bases, with 25 kN axial load, under cyclic bending in down-aisle direction, connected to a concrete deck or bolted-and-welded to a steel deck

the response of the bolted-and-welded specimens is superior when bolts are in tension, but is comparable in terms of load carrying and rotation capacity with that of specimens connected to the concrete floor when bolts are in the compression zone, despite a much higher energy dissipation capacity evidenced by the shape of the hysteresis loops.

Figures 2.75 and 2.76 compare the response of specimens simply bolted to a steel and to a concrete deck, under 25 kN axial load, respectively under bending in cross-aisle and in down-aisle direction.

The response of the specimens bolted to a steel deck is similar to that of the specimens bolted to a concrete floor, in the case of cross-aisle bending, with bolts in tension. When the bending direction is reversed, and bolts are in the compression zone, the specimens connected to the concrete deck show higher load-carrying and rotation capacity (Fig. 2.75).

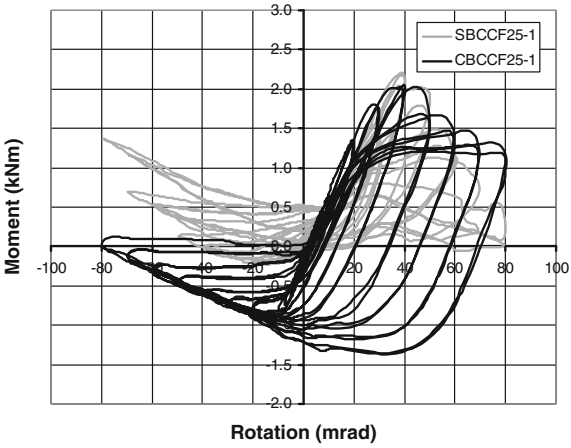

Fig. 2.75 Comparison of the hysteretic behaviour of column-bases, with 25 kN axial load, under cyclic bending in cross-aisle direction, bolted to a concrete or to a steel deck

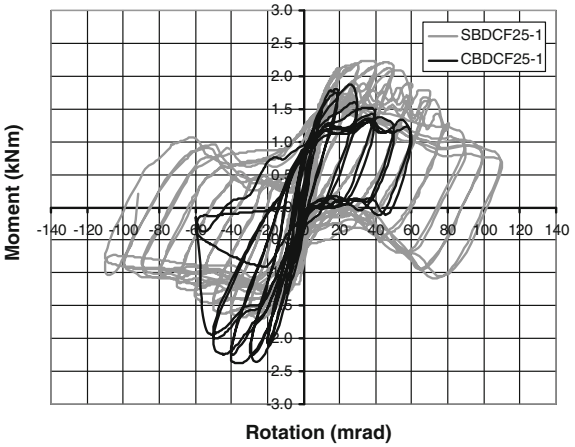

Fig. 2.76 Comparison of the hysteretic behaviour of column-bases, with 25 kN axial load, under cyclic bending in down-aisle direction, bolted to a concrete or to a steel deck

In down-aisle direction, specimens connected to a steel deck show a larger rotation capacity than those connected to a concrete floor. However, under bending with bolts in the compression zone, the load-carrying capacity of specimens connected to a concrete floor is higher.

Table 2.23 summarizes these type of comparisons, in terms of ratios of the main response parameters (yield moment M_y and rotation ϕ_y, initial elastic stiffness $S_{j,ini}$ number of plastic cycles to failure N_u and total absorbed energy E_{tot}) of the various specimens.

Figures 2.77, 2.78, 2.79 and 2.80 compare the main response parameters versus the applied axial load for specimens tested under cyclic bending. Information is available for all six combinations of floor connection and bending directions only in the case of 25 kN axial load. In fact, tests with higher values of the applied axial load were carried out only on specimens connected to a concrete floor.

Figure 2.77 shows that the yield moment of specimens connected to a concrete floor diminishes when increasing the axial load, for bending in cross-aisle direction, while for bending in down-aisle direction presents a maximum value corresponding to an axial load of 50 kN while, under 75 kN axial load, M_y is comparable with the one assessed under 25 kN axial load. Specimens bolted-and-welded to the steel floor show highest values of M_y for both bending directions, while the lowest value is associated to specimens bolted to a steel deck, under cross-aisle bending.

Figure 2.78 shows that the yield rotation of specimens connected to a concrete floor always diminishes when increasing the axial load. ϕ_y is however more influenced (in a negative sense) by the axial load when the specimen is under bending in cross-aisle direction.

Specimens bolted-and-welded to the steel floor show the highest values of ϕ_y for bending in cross-aisle direction, but also the lowest (together with the specimens simply bolted to a steel deck) under down-aisle bending.

Table 2.23 Comparison of results of cyclic tests on column-bases

M_y	ϕ_y	$S_{j,ini}$	N_u	E_{tot}	
(a) Steel base					
1.34	0.75	1.79	2.50	6.98	sbdcf25 /sbccf25
0.73	0.76	0.96	0.67	0.38	sbccf25 /cbccf25
1.11	0.72	1.53	2.50	4.29	sbdcf25 /cbdcf25
(b) Concrete base					
0.88	0.79	1.12	0.67	0.62	cbdcf25 /cbccf25
2.36	1.24	1.89	1.22	1.89	cbdcf50 /cbccf50
0.17	0.37	0.47	3.00	13.99	cbdcf75 /cbccf75
0.46	0.39	1.18	0.75	0.49	cbccf50 /cbccf25
1.24	0.62	2.00	1.38	1.48	cbdcf50 /cbdcf25
0.34	0.34	0.99	0.22	0.04	cbccf75 /cbccf50
0.83	0.74	1.13	0.55	0.33	cbdcf75/cbdcf50
0.16	0.13	1.18	0.17	0.02	cbccf75 /cbccf25
1.03	0.46	2.25	0.75	0.48	cbdcf75 /cbdcf25
(c) Athens base (bolted + welded)					
0.91	0.47	1.95	1.40	1.21	asbdcf25 /asbccf25
1.95	1.65	1.19	1.25	3.54	asbccf25 /sbccf25
1.32	1.03	1.29	0.70	0.61	asbdcf25 /sbdcf25
1.42	1.25	1.13	0.83	1.35	asbccf25/cbccf25
1.47	0.74	1.97	1.75	2.63	asbdcf25/cbdcf25

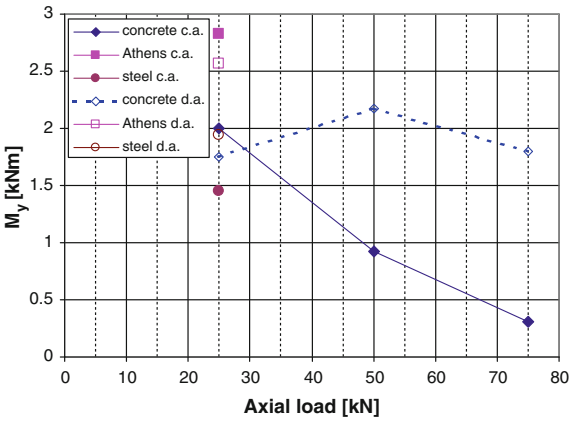

Fig. 2.77 Yield moment versus axial load

Figure 2.79 shows that the initial elastic bending stiffness $S_{j,ini}$ of specimens connected to a concrete floor always increases when increasing the axial load.

Specimens bolted-and-welded to the steel floor show the highest values of $S_{j,ini}$ for bending in down-aisle direction. Stiffness $S_{j,ini}$ of specimens connected to a concrete floor (under both bending directions) is similar and comparable with those

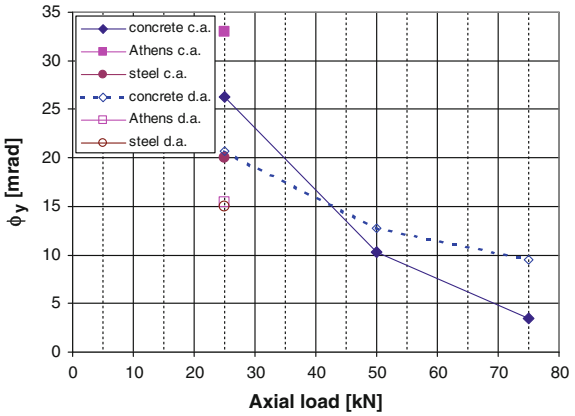

Fig. 2.78 Yield rotation versus axial load

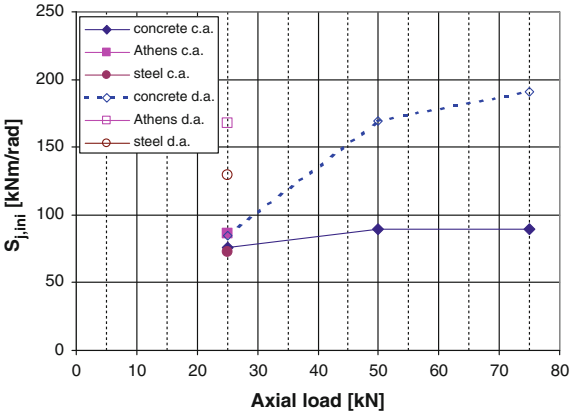

Fig. 2.79 Initial elastic stiffness versus axial load

of specimens simply bolted and bolted-and-welded under bending in cross-aisle direction.

Figure 2.80 shows that the number of cycles to failure for specimens under cross-aisle bending always diminishes when increasing the axial load while, under down-aisle bending, attains a maximum for an applied axial load of 50 kN. The specimen that sustained the largest number of plastic cycles was that bolted to a steel floor under down-aisle bending. Specimen simply bolted to a steel deck under cross-aisle bending and simply bolted to a concrete slab under down-aisle bending exhibited the same number of plastic cycles to failure.

The trend of the total absorbed energy E_{tot} is similar to the one of N_u as shown in Fig. 2.81. E_{tot} for specimens under cross-aisle bending always diminishes when increasing the axial load while, under down-aisle bending, attains a maximum for an applied axial load of 50 kN. The specimen that could absorb the largest amount

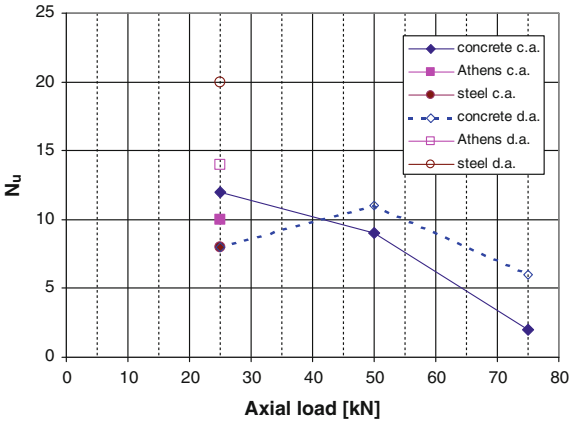

Fig. 2.80 Number of plastic cycles to failure versus axial load

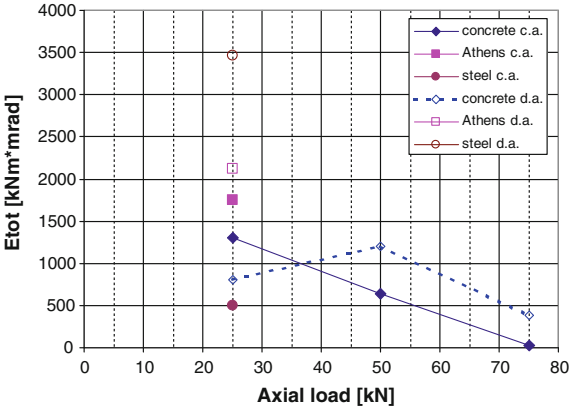

Fig. 2.81 Total absorbed energy versus axial load

of energy was the one bolted to a steel floor under down-aisle bending. Specimen simply bolted to a steel deck under cross-aisle bending exhibited the lowest energy absorption capacity.

Figure 2.82 shows the trend of the energy absorption capacity in terms of the ratio W_i/W_0 versus the number of cycles in the plastic range applied to the specimen, where W_i is the ratio of the energy absorbed in *i*th cycle to the energy absorbable in the same cycle by an elastic perfectly-plastic specimen, while W_0 is the ratio of the energy absorbed in the 1st cycle in the plastic range to the energy absorbable in the same cycle by an elastic perfectly-plastic specimen.

It can be noticed that all specimens show a similar trend of W_i/W_0, that abruptly drops (loosing approximately 40-60 % of energy dissipation capacity) in the first three or four plastic cycles, and then stabilizes until failure.

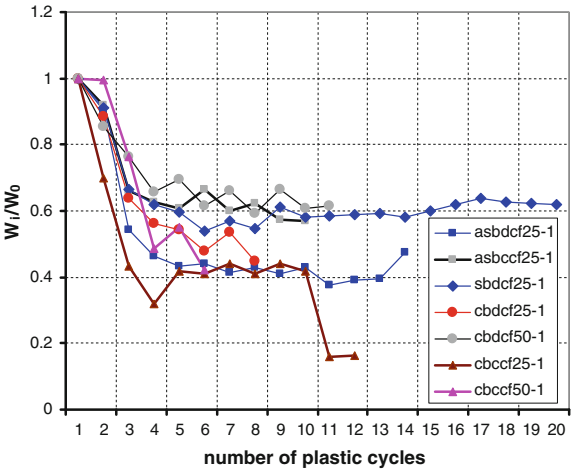

Fig. 2.82 Energy absorption capacity W_i/W_0 versus number of cycles in the plastic range

2.3.4 Conclusions

In the column base connection tests under cross-aisle bending, the axial compression load proved to be beneficial when the bolts are in the compression zone. In this case, an increase of the axial force results in an increase of resistance and stiffness, but in a decrease of rotation capacity of the specimens.

When the loading direction results in tension in the bolts, the axial compression load causes a reduction of resistance and stiffness of the column bases, because induces distortional buckling of the free edges of the cross-section profile.

The tests performed on the column base in the down-aisle direction proved that the axial compression load (25 and 50 kN) increases the initial stiffness and the resistance but decreases the rotation capacity of the connection.

In the cyclic tests, the higher the axial compression force, the bigger the difference between the resistance under positive and negative bending moments.

The collapse modes exhibited by the specimens were weld failure, base bending and distortion buckling of the cross section of the upright. In some tests premature weld failure caused a reduction in the rotation capacity of the connection. Therefore, it is extremely important to control the welding process during the manufacturing of the components.

Distortion buckling of the cross section of the upright occurred in the tests with an axial compression force of 50 and 75 kN, except for the monotonic test when the loading direction is such that bolts are in the compression zone. In the tests in cross-aisle direction with axial force of 75 kN distortion buckling occurred prematurely, drastically reducing the mechanical properties of the connection.

The base welded-and-bolted to a steel deck exhibited an increase of resistance and rotation capacity of the connection since there was no base plate bending. In the cyclic tests a higher capacity of energy dissipation was observed, when compared to simply bolted connections.

The results prove that connecting the column base to a concrete slab or to a steel deck does not substantially change the mechanical properties or the failure mode of the connection.

In both cases, however, pre-tension in the bolts should be provided.

References

ACI. (1999). *Acceptance criteria for moment frames based on structural testing*. Farmington Hills: American Concrete Institute, ACI, 374.

ATC-24. (1992). *Guidelines for cyclic testing of components of steel structures*. Redwood City, CA: Applied Technology Council.

Bernuzzi, C., Calado, L., & Castiglioni, C. A. (1997a). Ductility and load carrying capacity prediction of steel beam-to-column connections under cyclic reversal loading. *Journal of Earthquake Engineering, 1*(2), 401–432.

Bernuzzi, C., Calado, L., & Castiglioni, C. A. (2000). Low cycle fatigue of structural steel components: a method for re-analysis of test data and a design approach based on ductility. *Indian Society of Earthquake Technology (ISET), Special Issue on Experimental Techniques* (pp. 47–63), December.

ECCS. (1986). *Recommended testing procedure for assessing the behaviour of structural elements under cyclic loads*. European Convention for Constructional Steelworks, Publication No. 45.

Proença, J., Calado, L., & Ferreira, J. (1994). Some case studies of cyclic tests in RC and steel structural subassemblages. In S. Gomes et al. (Eds.), *Recent advances in experimental mechanics.* Balkema. *Proceedings of the 10th International Conference on Experimental Mechanics* (pp. 495–500), Lisbon.

Further Readings

Agatino M. R., Bernuzzi, C., & Castiglioni C. A. (2001). Joints under cyclic reversal loading in steel storage pallet racks. In *Proceedings. XVIII C.T.A. Conference, Venezia* (Vol. 2, pp. 105–114).

AS4084. (1993). *Steel storage racking*. Standards Australia.

Baldassino, N., Berardi, C., & Bernuzzi, C. (2001). Influence of the bracing systems on the performance of steel storage pallet racks. In *Proceedings of XVIII Conference C.T.A.* Venezia (pp. 115–125).

Baldassino, N., & Bernuzzi, C. (2000). Analysis and behaviour of steel storage pallet racks. *Thin-Walled Structures, 37*(4), 277–304.

Baldassino, N., Bernuzzi, C., & Zandonini R. (1999). Structural analysis of steel storage pallet racks. In *Proceedings of the 6th International Colloquium on Stability and Ductility of Steel Structures (SDSS'99)*, Timisoara, Romania (pp. 465–475).

Baldassino, N., Bernuzzi, C., & Zandonini R. (2000). Performance of joints in steel storage pallet racks. In *Proceedings of Connections in Steel Structures IV: Steel Connections in the New Millennium, Roanoke, Virginia, USA.*

Baldassino, N., Bernuzzi, C., Zandonini, R., & Hancock, G. (1998). Overall, local and distortional buckling in pallet racks. In *Proceedings of the Structural Stability Research Council Conference (S.S.R.C.)*, September, Atlanta U.S.A.

Baldassino, N., & Hancock, G. (1999). Distortional buckling of cold-formed steel storage rack sections including perforations. In P. Makelainen, P. Hassinen (Eds.), *Proceedings Fourth*

International Conference on Steel and Aluminium Structures (ICSAS'99), Helsinky (pp. 131–138). Oxford: Elsevier.

Baldassino, N., & Zandonini R. (2001). Numerical and experimental analysis of base-plate connections of steel storage pallet racks. In *Proceedings of XVIII Conference C.T.A.* (127–136), Venezia.

Baldassino, N., & Zandonini, R. (2002). Design by testing of steel storage pallet racks. In *Proceedings Of EUROSTEEL—3rd European Conference on Steel Structures*, Coimbra, Portugal.

Baldassino N., & Zandonini R. (2003). Industrial steel racks: tests, design and Codes. In *Proceedings ASSCCA'03 Advanced in Structures Steel, Concrete, Composite and Aluminium,* Sidney, Australia.

Baldassino N., & Zandonini R. (2004). Performance of base-palte connections of steel storage pallet racks. In D. Dubina & D. Grecea (Eds.), *Recent advances and new trends in structural design* (pp. 11–20). Timisoara: Editura Orizonturi Universitare. *Proceedings Of International Colloquium Dedicated to the 70th Anniversary of Professor Victor Gioncu,* Timisoara, May 7–8, 2004.

Ballio, G., Bernuzzi, C., & Castiglioni, C. A. (1999). An approach for the seismic design of steel storage pallet racks, spec. In *Stahlbau*, November.

Ballio, G., Calado, L., & Castiglioni, C. A. (1997). Low cycle fatigue and fracture of structural steel members and connections. *Fatigue and Fracture of Engineering Materials and Structures, 20*(8), 1129–1146.

Ballio, G., & Castiglioni, C. A. (1994). Seismic behavior of steel sections. *Journal of Constructional Steel Research, 29*, 21–54.

Ballio, G., & Castiglioni, C. A. (1995). A unified approach for the design of steel structures under low/or high cycle fatigue. *Journal of Constructional Steel Research, 43*(1995), 75–101.

Bernuzzi, C., Calado, L., & Castiglioni C. A. (1997b). Steel beam-to-column connections: failure criteria and cumulative damage models. In *Proceedings of the STESSA Conference, Kyoto* (pp. 538–545).

Bernuzzi, C., Calado, L., & Castiglioni, C. A. (1997c). Behaviour of steel beam-to-column joints under cyclic reversal loading: an experimental study. In *Proceedings of the 5th International Colloquium on Stability and Ductility of Steel Structures, SDSS, Nagoya* (Vol. 1, pp. 335–342).

Bernuzzi, C., Calado, L., & Castiglioni C. A. (1998). Structural steel components under low-cycle fatigue: Design assisted by testing. In *Proceedings of the SEWC, San Francisco.*

Bernuzzi, C., & Castiglioni, C. A. (2001). Experimental analysis on the cyclic behaviour of beam-to-column joints in steel storage pallet racks. *Thin-Walled Structures, 39*, 841–859.

Bernuzzi, C., & Zandonini, R. (1993). *Serviceability and analysis models of steel buildings*. Goteborg, Sweden: International Colloquium on Structural Serviceability of Buildings.

Bernuzzi, C., Zandonini, R., & Zanon, P. (1991). Rotational behaviour of extended end plate. *Costruzioni Metalliche, 43*(2), 74–103.

Brescianini, J. C., Castiglioni, C. A., & Panzeri, N. (2003). Dynamic experimental tests on steel pallet racks. In *Proceedings of CTA, Genova* (pp. 107–116).

Calado, L., & Castiglioni, C. A. (1995). Low-cycle fatigue testing of semi-rigid beam-to-column connections. In *Proceedings Of 3rd International Workshop on Connections in Steel Structures, IABSE/AISC, Trento.*

Calado, L., & Castiglioni, C. A. (1996). Analise experimental do comportamento ciclico de ligacoes metalicas viga-pilar. *Mecanica Experimental, 1*, 61–72.

Calado, L., Castiglioni, C. A., & Bernuzzi, C. (1998). Behaviour of steel beam-to-column joints under cyclic reversal loading: An experimental study. In T. Usami & Y. Itoh (Eds.), *Stability and ductility of steel structures* (pp. 279–292). Amsterdam: Elsevier Science Ltd.

Calado, L., Castiglioni, C. A., Mele, E., & Ferreira, C. (1999). Damage accumulation design of steel beam-to-column connections. In *Proceedings of the 2nd Encontro Nacional de Construção Metalica e Mista, Coimbra* (pp. 551–563).

Castiglioni, C. A. (1994). Effects of local buckling on the cyclic behavior of steel members. In *S.S. R.C. 50th Anniversary Meeting, Bethlehem, PA, June 1994, Proceedings of the Technical Session* (pp. 381–395).

Castiglioni, C. A. (1995a). Seismic damage assessment of steel members and joints. In *SSRC, Theme Conference on Stability Problems related to aging, damaged and deteriorated structures, Kansas City* (pp. 55–66).

Castiglioni, C. A. (1995b). Seismic behavior of steel beam-column members. In *SSRC, Theme Conference on Stability Problems related to aging, damaged and deteriorated structures, Kansas City* (pp. 77–88).

Castiglioni, C. A. (1999). Failure criteria and cumulative damage models for steel components under low-cycle fatigue. In *Proceedings XVII C.T.A. Conference, Napoli.*

Castiglioni, C. A. (2003a). Dynamic tests on steel pallet racks. *Costruzioni Metalliche, 55*(3), 35–44.

Castiglioni, C. A. (2003b). Seismic behaviour of steel storage racks. In *Proceedings of the IV Congresso de Construcao Metalica e Mista, Lisbon* (pp. 41–62), December 4–5, 2003.

Castiglioni, C. A. (2005). Effects of the loading history on the local buckling behavior and failure mode of welded beam-to-column joints in moment-resisting steel frames. *Journal of Engineering Mechanics, ASCE, 131*(6), 568–585.

Castiglioni, C. A., Bernuzzi, C., Calado, L., & Agatino, M. R. (1997). Experimental study on steel beam-to-column joints under cyclic reversal loading. In *Proceedings Of the Northridge Earthquake Research Conference, Los Angeles* (526–533).

Castiglioni, C. A., Brescianini, J. C., & Panzeri, N. (2003a). Variable Amplitude, low-cycle fatigue testing of welded steel beam-to-column joints. *Costruzioni Metalliche, 55*(2), 35–51.

Castiglioni, C. A., & Calado, L. (1996). Seismic damage assessment and failure criteria for steel members and connections. *Proceedings of the International Conference on Advances in Steel Structures, Hong Kong, II*, 1021–1026.

Castiglioni, C. A., Mouzakis, H., & Carydis, P. (2007). Constant and variable amplitude cyclic behaviour of welded steel beam-to-column connections. *Journal of Earthquake Engineering, 11*(6), 876–902.

Castiglioni, C. A., Panzeri, N., Brescianini, J. C., & Carydis, P. (2003b). Shaking table tests on steel pallet racks. In *Proceedings STESSA 2003, Napoli* (pp. 775–781).

CEB. (1996). *RC frames under earthquake loading—State of the art report*. Comité Euro-International du Beton, Thomas Telford Ed.

CEN. (2005). *Eurocode 3: Design of Steel Structures—Part 1.1 general rules and rules for buildings*. European Committee for Standardization.

Chen, C. K. (1980). *Seismic study on industrial steel storage racks*. Prepared for the National Science Foundation, URS/ John A. Blume & Associate Engineers, June.

Davies, M., & Jiang, C. (1998). Design for distorsional buckling. *Journal of Constructional Steel Research, 46*(1–3), 174–175.

ECCS. (1992). *Analysis and design of steel frames with semi-rigid joints*. European Convention for Constructional Steelworks, Publication n. 67.

FEM 10.2.02. (2000). *The design of static steel pallet racks*. Federation Europeen de la Manutention, Vers. 1.01.

FEM 10.2.08. (2005). *The seismic design of static steel pallet racks*. Federation Europeen de la Manutention, Final draft, December 2005.

FEMA. (2005). *Seismic Considerations for Steel Storage Racks Located in Areas Accessible to the Public. FEMA 460,* September 2005.

Godley, M. H. R. (1991). Storage racking, Chapter 1. In Rhodes (Ed.), *Design of cold formed steel members* (pp. 361–399). London, UK: Elsevier Applied Science.

Hancock, G. J. (1985). Distortional buckling of steel storage rack columns. *Journal of Structural Engineering, ASCE, 111*(12), 2770–2783.

Markazi, F. D., Beale, R. G., & Godley, M. H. R. (1997). Experimental analysis of semi-rigid boltless connectors. *Thin-Walled Structures, 28*(1), 57–87.

Mazzolani, F. M., & Piluso V. (1996). *Theory and design of seismic resistant steel frames*. London: Champmann and Hall, E&FN Spon.

Proença, J., Calado, L., Castiglioni, C. A., & Tristão G. (2006). Cyclic testing on steel storage beam-to-upright subassemblages. An innovative cyclic testing procedure. In *1st European Conference on Earthquake and Seismology, Geneva*, paper n. 1152.

RAL. (1990). *Storage and associated equipment*. RAL Deutsches Institut fur Gutersicherung und Kennzeichnung (German Institute for Quality Assurance and Marketing).

RMI. (1990). *Specification for the design testing and utilization of industrial steel storage racks*. Charlotte, NC: Rack Manufacturers Institute, 1990 edition.

RMI. (1997). *Specification for the design, testing and utilization of industrial steel storageracks*. Charlotte, NC: Rack Manufactures Institute.

RMI. (2002a). *Specification for the design testing and utilization of industrial steel storage racks*. Charlotte, NC: Rack Manufacturers Institute, 2002 edition.

RMI. (2002b). *Commentary to specification for the design testing and utilization of industrial steel storage racks.* Charlotte NC: Rack Manufacturers Institute.

RMI. (2004). *Testing guidelines for pallet stacking frames*. Charlotte, NC: Rack Manufacturing Institute.

Zandonini, R., Baldassino, N., & Bernuzzi, C. (1998). Experimental and numerical studies on pallet racks. In *Proceedings of the Conference "Professor Otto Halase-Memorial Session"*, Budapest TU, Budapest, Rumania.

Zandonini, R., Baldassino, N., & Bernuzzi, C. (1999a). Structural analysis of steel storage pallet racks. In D. Dubina, & M. Ivanyi (Eds.), *Proceedings Of Stability and Ductility of Steel Structures (SDSS'99)* (pp. 465–475), Timisoara, Rumania. Oxford: Elsevier.

Zandonini, R., Baldassino, N., & Bernuzzi, C. (1999b). Influence of beam-to-column joint modelling on the performance of steel pallet racks. In G. Huber, T. Michl (Ed.), *Festschrift Commemorative Publication Prof. Dr. Ferdinand Tschemmernegg* (pp. 351–363). Innsbruck: Institut fur Stahlbau, Holzbau und Mischbautechnologie.

Zandonini, R., Baldassino, N., Bernuzzi, C., & Hancock, G. (1998). Overall, local and distortional buckling in pallet racks. In *Proceedings of the Structural Stability Research Council,(S.S.R.C.)*, Atlanta, GA, September 1998.

http://www.springer.com/978-3-319-28465-1

Seismic Behavior of Steel Storage Pallet Racking Systems

Castiglioni, C.A.

2016, XLVI, 461 p. 475 illus., 253 illus. in color.,
Hardcover
ISBN: 978-3-319-28465-1